CHAPTER VII

FISCHER-TROPSCH SYNTHESIS: COMPARISONS BETWEEN Pt AND Ag PROMOTED Co/Al_2O_3 CATALYSTS FOR REDUCIBILITY, LOCAL ATOMIC STRUCTURE, AND CATALYTIC ACTIVITY

7.1 Abstract

For economic reasons, Ag as a substitute for Pt promoter for FT Co/Al_2O_3 catalysts was advocated, due to its satisfactory ability to facilitate cobalt oxide reduction, its good catalytic performance in improving the CO conversion and selectivity and, especially, its much lower price compared to that of Pt (i.e., \$23.31/Troy oz Ag. vs \$1486.0/Troy oz Pt. (May 10th 2013)). A comparative study between Pt and Ag promoters at several equivalent atomic loadings was performed in this work. While either Pt or Ag significantly facilitates cobalt oxide reduction supplying additional Co metal active sites compared to the unpromoted Co/Al_2O_3 catalysts, the total metal site density increased with increasing Pt loading, but become attenuated at high Ag loading. The EXAFS results indicate isolated Pt atoms interact with cobalt cluster to form Pt-Co bonds, without evidence of Pt-Pt bond formation, even at levels as high as 5 wt % Pt. In Ag promoted Co/Al_2O_3 catalyst, not only were Ag-Co bonds observed, but Ag-Ag bonds were present, even at levels as low as 0.276% Ag. The degree of Ag-Ag coordination increased as a function of Ag loading, while decreases in BET surface area and a shift to wider average pore size suggests some pore blocking by Ag at high loadings, which likely blocked access of reactant to internal cobalt sites. Therefore, although both promoters initially facilitate reduction of cobalt oxides, their local atomic structures are fundamentally different. Either Pt or Ag can significantly improve the CO conversion rate on a per gram catalyst basis of Co/Al_2O_3. Slightly adverse effects on selectivity (i.e., increased CH_4 and CO_2, at detriment to C_5+) were found with Pt, especially at higher loading, while Ag provides some benefits (i.e., slightly decreases CH_4 and CO_2, and increases C_5+) at all loadings tested in this work.

Keywords: Fischer-Tropsch synthesis (FTS), gas-to-liquids (GTL), silver (Ag), platinum (Pt), cobalt (Co), Co/Al_2O_3, XANES, EXAFS, oxidation-reduction (OR) cycles

7.2 Introduction

Cobalt/alumina is an effective Fischer-Tropsch synthesis (FTS) catalyst for gas-to-liquids (GTL) production from syngas with high H_2/CO ratio (~2:1). There is general agreement that reduced Co metal surface sites are active sites for Fischer-Tropsch synthesis over this catalyst. Unlike other metals typically employed in catalysis, cobalt on alumina for FTS is often loaded in high amounts, often at or exceeding 20% by weight. Because the alumina support interacts strongly with cobalt (Espinoza, 1998; Van Berge et al., 2001), higher loadings facilitate the reduction of cobalt oxide species during activation and make the catalyst more resistant to deactivation (e.g., by oxidation at high conversion) (Espinoza, 1998; Van Berge et al., 2001). Despite high Co metal loadings, the support still hinders the ability of cobalt oxide to be reduced during thermal activation in H_2 at moderate temperature (e.g., 350 °C for 10 h in H_2).

The addition of noble metal promoters (e.g., Pt, Ru, and Re) (Arnoldy et al., 1985; Christensen et al., 2009; Das et al., 2003; Hilmen et al., 1996; Jacobs et al., 2004; Jacobs et al., 2002; Kogelbauer et al., 1996; Rønning et al., 2001; Schanke et al., 1995; Vada et al., 1995; Van Berge et al., 2001) significantly enhances the reducibility of cobalt oxide interacting with the alumina support and, consequently, provides additional Co metal sites densities for the reaction in comparison with the unpromoted catalyst. A H_2 dissociation and spillover mechanism (Jacobs et al., 2004; Jacobs et al., 2002; Jacobs et al., 2009) was believed to be a possible way of promotion, in which the promoter metal, first reduced at lower temperature such that H_2 dissociated and spilled over from the metal promoter to form nuclei of Co^0 in the cobalt oxide, with this reduced cobalt expediting further reduction of cobalt oxide particles. Among these noble metal promoters, Pt promoter is among the most widely used in commercial FT Co/Al_2O_3 catalysts. PtO_2 has been observed after calcination (Weaver et al., 2005), while only a Pt-Co bimetallic phase was found in

the Pt-Co/Al_2O_3 catalyst (Cook et al., 2012; Guczi et al., 2002; Jacobs et al., 2004) after activation in H_2, as investigated by EXAFS spectroscopy. This structural coordination was suggested to be responsible for facilitating Co reduction and thereby improving the CO conversion rate on a per gram catalyst basis.

Group 11 metals (Cu, Ag, Au) has been investigated as potential substitutes for Pt (Jacobs et al., 2009), due to their ability to facilitate reduction of cobalt oxides and, in particular, due to the lower prices of Ag and Cu compared to that of noble metals like Pt. We found that although all the Group 11 metals enhanced the reducibility of cobalt oxides and increased the fraction of Co reduced, there were differences in catalytic activity and selectivity: introducing Ag or Au (the latter at lower levels) improved CO conversion and slightly improved reaction selectivity relative to the unpromoted catalyst, while adding Cu, the catalytic activity and selectivity were worse than those of the unpromoted catalyst. Because of the good performance of Ag in facilitating cobalt reduction and in performance together with its lower price compared with Au, Ag appears to be the best among Group 11 metals and to be the most promising promoter as a substitute for platinum, a promoter used commercially. Well dispersed Ag_2O was suggested to be the main Ag species in a Ag-Co/Al_2O_3 catalyst after calcination or oxidation (Jacobs et al., 2009; Kuzmin et al., 2006) and this species quickly reduced during activation conditions (Greenwood, 1997). In our preliminary study of the local atomic structure of Ag-Co/Al_2O_3 catalyst Ag-Co coordination was difficult to assess due to the high loading of Ag used (Jacobs et al., 2009). Notwithstanding, because of the ability of Ag to facilitate Co reduction and to slightly reduce CH_4 formation as observed in our recent work (Jacobs et al., 2009), Ag-Co coordination is expected to be detected at lower Ag loadings, and this was investigated in this work using the EXAFS technique and scanning at the Ag K-edge. Adding Ag to hydrogenating catalysts can hinder the hydrogenation reaction and Ag-active metal bimetallic was proposed to be an active site (Redjala et al., 2006). This could shed lighten why CH_4 selectivity is decreased in the Ag promoted Co FT catalyst.

A comparative study between Pt and Ag was conducted in this work. Although proposed in our previous report about the role of Pt (Jacobs et al., 2004) and Ag (Jacobs et al., 2009) promoter, one objective of this work was to determine if

additional levels of loading could further facilitate cobalt reduction, and find the point at which Pt-Pt bonds could be identified in the case of Pt promotion or the point at which Ag-Co could be found in the case of Ag, which were not disclosed before; moreover, the most appropriate Pt and Ag loading will be suggested. In so doing, different levels of atomically equivalent loadings of Pt or Ag were applied to 25%Co/Al_2O_3. Standard characterization methods (e.g., H_2 TPR, H_2 chemisorption/oxygen pulse reoxidation, X-ray diffraction, and BET) were also employed. The catalysts were thoroughly characterized at the atomic level by EXAFS spectroscopy, while electronic information was also obtained by XANES. Moreover, CSTR tests were implemented at ~50% conversion level so that FTS selectivities could be directly compared between Pt and Ag promoted cobalt catalysts.

7.3 Experimental

7.3.1 Catalyst Preparation

The catalyst support used was Sasol Catalox-150 γ-Al_2O_3. To achieve 25%Co loading, a slurry impregnation method, which follows a Sasol patent (Espinoza, 1998), was used. Cobalt nitrate hexahydrate ($Co(NO_3)_2 \cdot 6H_2O$) (Alfa Aesar) was employed to make the Co precursor solution. The ratio of the volume of loading solution used to the weight of alumina was 1:1, such that approximately 2.5 times the pore volume of solution was used. Two impregnation steps of cobalt nitrate were applied. Between each step the catalyst was dried under vacuum in a rotary evaporator. After the last step of cobalt addition, platinum or silver precursor solution was added to the Co/Al_2O_3 catalyst by incipient wetness impregnation. Tetra-amine platinum (II) nitrate solution and silver nitrate (Alfa Aesar) were utilized as Pt and Ag sources, respectively. A series of Pt promoted Co/Al_2O_3 catalysts was prepared with loadings of 0.5%, 1%, 2%, 3%, 4%, and 5%, which are atomically equivalent to Ag loadings of 0.276%, 0.553%, 1.11%, 1.66%, 2.21%, and 2.76%, respectively. Only after the final step were catalysts calcined under air flow at 350 °C for 4 h.

7.3.2 BET Surface Area and Porosity Measurements

The measurements of BET surface area and porosity of the calcined catalysts were conducted using a Micromeritrics Tri-Star system. Before performing the test, the temperature was gradually ramped to 160 °C and the sample was evacuated at least 12 h to approximately 50 mTorr. The BET surface area, pore volume (single point), and average pore radius (single point and BJH adsorption) were obtained for each sample.

7.3.3 Temperature Programmed Reduction (TPR)

Temperature programmed reduction (TPR) profiles of calcined catalysts were recorded using a Zeton-Altamira AMI-200 unit equipped with a thermal conductivity detector (TCD). Samples were pretreated by purging with argon flow at 350 °C to remove traces of water. The TPR was performed using a 10%H_2/Ar gas mixture and referenced to argon at a flow rate of 30 cm^3/min. The sample was heated from 50 to 800 °C using a heating ramp of 10 °C/min.

7.3.4 H_2 Chemisorption and Percentage Reduction by Pulse Reoxidation

Hydrogen chemisorption was conducted at using temperature programmed desorption (TPD), also measured with the Zeton-Altamira AMI-200 instrument. The sample weight was typically ~0.220 g. Catalysts were activated in a flow of 10 cm^3/min of H_2 mixed with 20 cm^3/min of argon at 350 °C for 10 h. and then cooled under flowing H_2 to 100 °C. The sample was held at 100 °C under flowing argon to remove and/or prevent adsorption of weakly bound species prior to increasing the temperature slowly to 350 °C, the reduction temperature of the catalyst. The catalyst was held under flowing argon to desorb remaining chemisorbed hydrogen until the TCD signal returned to baseline. The TPD spectrum was integrated and the number of moles of desorbed hydrogen determined by comparing its area to the areas of calibrated hydrogen pulses. The loop volume was first determined by establishing a calibration curve with syringe injections of hydrogen in helium flow. Dispersion calculations were based on the assumption of a 1:1 H:Co stoichiometric ratio and a spherical cobalt cluster morphology. After TPD of

hydrogen, the sample was reoxidized at 350 °C using pulses of oxygen. The percentage of reduction was calculated by assuming that metal reoxidized to Co_3O_4. Further details of the procedure are provided elsewhere (Jacobs et al., 2002).

7.3.5 X-ray Diffraction (XRD)

Powder diffractograms on calcined catalysts were recorded using a Philips X'Pert diffractometer. Two different tests were performed for each sample — a short time scan over a long range and a long time scan over a short range. The objective of the short time scan was to assess the crystalline phases present using the following conditions: scan rate of 0.02 °/step and scan time of 5 s/step over a 2θ range of 15-80°. The long time scan was conducted to quantify average Co_3O_4 domain sizes using line broadening analysis for the peak at 2θ = 37° representing (311). The latter conditions employed were a scan rate of 0.01 °/step and a scan time of 30 s/step over a 2θ range of 30-45°.

7.3.6 Extended X-ray Absorption Fine Structure (EXAFS) and X-ray Absorption Near Edge (XANES) Spectroscopies

In situ H_2-TPR XAFS studies were performed at the Materials Research Collaborative Access Team (MR-CAT) beamline at the Advanced Photon Source, Argonne National Laboratory. A cryogenically cooled Si(111) monochromator selected the incident energy and a rhodium-coated mirror rejected higher order harmonics of the fundamental beam energy.

The experiment setup was similar to that outlined by Jacoby (Jacoby, 2001). A stainless steel multi-sample holder (3.0 mm i.d. channels) was used to monitor the in situ reduction of 6 samples during a single TPR run. Approximately 12.5 mg of each sample was loaded as a self-supporting wafer in each channel. The catalyst to diluent weight was approximately 0.1. Supported cobalt catalyst samples were diluted with sufficient SiO_2 to allow for the wafer to be a self-supporting. The holder was placed in the center of a quartz tube, equipped with gas and thermocouple ports and Kapton windows. The amount of samples used was optimized for the Pt L_{III}-edge and Ag-K edge, considering the absorption by Al and Si of the support. The samples were pretreated (to ensure dryness) off line in flowing air at 200 °C for

15 min, cooled down to room temperature and transferred into the experiment hutch. The quartz tube was placed in a clamshell furnace mounted on positioning table. Each sample cell was positioned relative to the beam by finely adjusting the position of the table to an accuracy of 20 μm (for repeat scans). Once the sample positions were fine-tuned, the reactor was purged with helium for more than 5 min at 30 ml/min then the reactant gas (H_2/He, 4%) was flowed through the samples (30 ml/min) and a temperature ramp of 0.7°C/min (starting from ~50 °C after a more rapid startup) was initiated for the furnace

The Pt L_{III}-edge spectra were recorded in transmission mode and a Pt metallic foil spectrum was measured simultaneously with each sample spectrum for energy calibration. X-ray absorption spectra for each sample were collected from 11632 – 12108 eV, with a step size of 10 eV and acquisition times of 30 min per scan. By measuring each sample, in turn, and repeating, this allowed 33 scans to be collected for each sample over a 16 hour and a half period. The sample's temperature change from the absorption edge through the end of the scan was then about 4.0 °C, while each sample was measured approximately every 22.6 °C. While the Ag K-edge spectra were also recorded in transmission mode and a Ag metallic foil spectrum was employed for energy calibration. X-ray absorption spectra were collected from 25266 – 26157 eV, with a step size of 15 eV and acquisition times of 30 min per scan. By measuring each sample, in turn, and repeating, this allowed 33 scans to be collected for each sample over a 16 h and a half period. The sample's temperature change from the absorption edge through the end of the scan was then about 3.5 °C, while each sample was measured approximately every 23.3 °C. After the sample temperature reached to 350 °C, the sample was then held at this temperature for 6 h 30 min and the scans were also done as function of time. Then, the catalyst samples were cooled down to room temperature and the final scans were performed.

XANES spectra were processed using the WinXAS program (Ressler, 1997). For the case of Pt promoted catalysts, simultaneous pre and post-edge background removal was carried out using degree 2 polynomial nomimals over the ranges 11.413-11.498 and 11.662-12.076 keV, respectively, and normalization by division of the height of the absorption edge. For Ag promoted catalysts, XANES

spectra were processed in the same manner but over the pre-edge range of 25.342-25.444 keV and the post-edge range of 25.615-25.122 keV with normalization. Once the spectra were processed, they were compared with reference compounds. For Pt-25%Co/Al_2O_3, all of the beginning spectra closely resemble the bulk PtO_2 reference compound. Therefore, the initial spectrum for each catalyst was used as the reference for PtO_2 in the sample. As the temperature trajectory was followed, it was clearly observed that a PtO_2 to PtO transition took place for all the samples, considering the white line intensities and the line shapes. Further following the temperature trajectory, the conversion from PtO to Pt^0 occurred. The catalyst spectra at 350 °C resemble the spectrum of Pt^0, so they were used as a Pt^0 reference. To specify the spectrum of PtO in the catalyst samples, which has a line shape similar to PtO_2 but with an attenuated intensity, a linear combination fitting was performed using PtO_2 and Pt^0 in samples as references. The spectrum composed of 50% PtO_2-50%Pt^0 was empirically selected as a PtO sample reference. Finally, a linear combination fitting was performed by using those 3 Pt reference compounds for analyzing spectra along the temperature trajectory. For Ag-25%Co/Al_2O_3 catalyst, the starting spectra of all samples did not resemble any bulk Ag compound references (i.e., AgO, Ag_2O). However, it has been previously suggested that Ag_2O was more likely to be a Ag species in calcined samples (Kuzmin et al., 2006). Along with the temperature trajectory, it was obvious that Ag_2O converted to Ag^0. Thus, a linear combination fitting was performed using Ag_2O and Ag^0 in the samples as references.

EXAFS spectra were also processed using WinXAS (Ressler, 1997). Initially, the catalysts were analyzed over the k-range 2-12 $Å^{-1}$. For those spectra, simultaneous pre and post-edge background removal was carried out with two polynomial degree 2 functions over the ranges 11.413-11.498 and 11.662-12.076 keV, respectively, for Pt promoted catalysts and over the ranges 25.342-25.444 and 25.615-25.122 keV, respectively, for Ag promoted catalyst. The spectra were normalized by dividing by the height of the edge jump. Spectra were then calibrated versus the Pt^0 or Ag^0 reference spectrum, and then converted to k-space. A cubic weighted degree 7 spline was used to remove the background of the $\chi(k)$ function. Finally, the data in k-space were Fourier transformed to R-space using a Bessel

window to obtain the radial distribution function (using a k^3-weighting for Pt promoted catalysts and k^1-weighting for Ag promoted catalysts). EXAFS fittings were carried out using the catalysts in their final state following TPR and cooling. All catalysts displayed high quality data over the k-range of 2-12 $Å^{-1}$ range. In R-space for Pt promoted catalysts, the first Pt-Co coordination shell was isolated by employing a Bessel window and then taking the back-Fourier Transform. After converting to $\chi(k)$, fitting of the spectra was carried out in k-space using FEFFIT (Newville, 2005). The k-range employed was 3-12 $Å^{-1}$. The FEFF program (Rehr et al., 1992)was used to construct a model of Pt-Co FCC to be used in fitting, and the atomic coordinates of Pt FCC (with lattice parameters) were inputted to the FEFF program with the aid of the program Atoms (Ravel, 2001). In order to use coordination number as a fitting parameter, the amplitude reduction factor S_0^2 must be fixed for all scattering paths in the solid, and it was assumed to be 0.9 by the zeroth order approximation. For Ag promoted catalysts, the first Ag-Co and Ag-Ag coordination shells in R-space were identified and also isolated by using a Bessel window and then back Fourier transformed to k-space. Fitting was performed over the k-range of 2-10 $Å^{-1}$. The model for Ag consisted of Ag-Co and Ag-Ag bonds generated by the FEFF and Atoms programs. The amplitude reduction factor S_0^2 of 0.9 was also applied.

7.3.7 Catalytic Activity Testing

FTS reaction tests were conducted using a 1 L CSTR equipped with a magnetically driven stirrer with turbine impeller, a gas-inlet line, and a vapor outlet line with a stainless steel (SS) fritted filter (7 μm) placed external to the reactor. A tube fitted with a SS fritted filter (2 μm opening) extends below the liquid level of the reactor for withdrawing reactor wax to maintain a nearly constant liquid level in the reactor. Separate mass flow controllers were used to control the flow of hydrogen and carbon monoxide at the desired flow rate. The reactant gases were premixed in a vessel before entering the reactor. Carbon monoxide was passed through a vessel containing lead oxide-alumina to remove traces of iron carbonyls. The mixed gases entered the CSTR below the stirrer operated at 750 rpm. The reactor slurry temperature was maintained constant by a temperature controller.

Prior to performing the reaction test, the catalyst (~13.0 g) was ground and sieved to 45-90 μm, and then loaded into a fixed-bed reactor for ex-situ reduction at 350 °C under atmospheric pressure for 15 h using a gas mixture of H_2/He (60 NL/h) with a molar ratio of 1:3. The reduced catalyst was then transferred to a 1 L continuously stirred tank reactor (CSTR) containing 315 g of melted Polywax 3000, by pneumatic transfer under the protection of a N_2 inert gas. Weighing the reactor before and after the transfer of catalyst was done to ensure that all catalyst powder was successfully transferred to the reactor. The transferred catalyst was further reduced in-situ at 230 °C at atmospheric pressure using pure hydrogen (30 NL/h) for another 10 h before starting the Fischer-Tropsch synthesis (FTS) reaction.

In this study, the FTS conditions used were 220 °C, 2.2 MPa, H_2/CO = 2.1. The reactant gas mixture was analyzed prior to sending to the reactor to ensure the composition. The reaction products were continuously removed from the vapor space of the reactor and passed through two traps, a warm trap maintained at 100 °C and a cold trap held at 0 °C. The uncondensed vapor stream was reduced to atmospheric pressure. The gas flow was measured using a wet test meter and analyzed by online GC. The accumulated reactor liquid products were removed every 24 h by passing through a 2 μm sintered metal filter located below the liquid level in the CSTR. Conversions of CO were obtained by gas-chromatography analysis (micro-GC equipped with thermal conductivity detectors) of the outlet gas product. The reaction products were collected in three traps maintained at different temperatures; a hot trap (200 °C), a warm trap (100 °C), and a cold trap (0 °C). The products were separated into different fractions (rewax, wax, oil, and aqueous) for quantification. However, the oil and wax fractions were mixed prior to GC analysis (Jacobs et al., 2009). To investigate the effect of Pt and Ag on the activity and selectivity, a reference CO conversion of about 50% was used and achieved by adjusting the space velocity in all cases. Activities were compared by adjusting space velocity and measuring the space velocity used to achieve 50%CO conversion, while selectivities were directly compared at the same level of conversion.

7.4 Results and Discussion

7.4.1 BET and Porosity Measurement

The results of surface area and porosity data as measured by N_2 physisorption at 77 K are shown in Table 7.1. Sasol Catalox-150 γ-Al_2O_3 was used as a catalyst support and its specific BET surface is 150 m^2/g. Because the analysis was taken for calcined catalysts, Co_3O_4 was deemed to be a major cobalt oxide compound in this catalyst (Jacobs et al., 2001). 34%Co_3O_4 by weight was calculated by assuming 25wt%Co metals in Co/Al_2O_3 catalyst were completely converted to Co_3O_4 after calcination. Thus, if Al_2O_3 is the only contributor to the area, then the area of 25%Co/ Al_2O_3 catalysts should be $150 \times 0.66 = 99$ m^2/g, which is very closed to the measured value of 98.4 m^2/g. Interestingly, Pt promoter seems to have an effect on the BET results, namely, increasing Pt loading evidently increases BET surface area and slightly decreases average pore radius. On the other hand, adding Ag promoter did not significantly alter the BET results of the catalyst, even at high Ag loadings.

7.4.2 Temperature Programmed Reduction

As observed in previous studies, the TPR profiles in Figure 7.1 show that either Pt or Ag promoter can significantly facilitate cobalt oxide reduction. As proposed in previous work (Jacobs et al., 2007), the TPR profile of a Co/Al_2O_3 catalyst is typically comprised of two main peaks; the first peak centered at around 320 °C representing the chemical change of Co_3O_4 to CoO and the another broader peak (about 3 times the area) situated at 590 °C expressing the subsequent conversion of CoO to metallic Co^0. In a typical TPR profile of both unpromoted and promoted Co/Al_2O_3 catalysts, the first peak is normally sharper than the second peak since the reduction of Co_3O_4 is facile regardless of either metal-support interaction or cluster size, while the subsequent reduction of CoO likely depends on cluster size, with the smaller more strongly interacting clusters being more difficult to reduce (Cook et al., 2012; Cronauer et al., 2012; Jacobs et al., 2002; Sexton et al., 1986; Vada et al., 1995; Van Berge et al., 2001; Wang et al., 1991). Besides the two prominent peaks presented in unpromoted Co/Al_2O_3 catalyst (bottom), a shoulder

peak on the second peak at around 700 °C was also observed. This peak was thought of as the smallest Co surface species, with the greatest interaction with the support, while some cobalt remains unreduced until even higher temperatures and is related to a small amount of cobalt that is sacrificed as cobalt aluminate (Jacobs et al., 2002).

Figure 7.1(A) shows the effect of Pt and Pt loading on TPR profiles. 0.5%Pt by weight forces the center of the first peak shift to ~175 °C (145 °C shift) and the second peak to 420 °C (170 °C shift) relative to the unpromoted Co/Al_2O_3 catalyst. Increasing Pt causes further decreases in the reduction temperatures of cobalt oxides, but with diminishing returns. In TPR profiles of 0.5%Pt and 1.0%Pt-25%Co/Al_2O_3 catalysts, a small peak at ~ 240 °C was observed as a low temperature shoulder of the second peak. To identify this peak, quantification of peak area was conducted. It was found that the area of this peak combined with the area of the second peak is ~ 3 times that of the first peak. Therefore, this small peak likely represents a fraction of CoO having a larger size and, in turn, a weaker interaction with the support. Recall that the stoichiometry of reduction is: $Co_3O_4 + H_2 = 3CoO + H_2O$ and $3CoO + 3H_2 = 3Co^0 + 3H_2O$. Similarly, the addition of 0.276%Ag (atomically equivalent to 0.5%Pt) also shifts both peaks to lower temperatures, to ~270 °C (50 °C shift) and to ~420 °C (170 °C shift) for the first and the second peaks, respectively. Compared with Pt, although Ag addition did not shift the first peak (left) to the low temperature achieved with Pt, interestingly, the shift of the second peak (right) is nearly the same. To complete cobalt oxide reduction to metal particles, reduction temperature used depends on the extent of reduction of the second peak ($CoO \rightarrow Co^0$). Thus, it can be concluded that Ag may serve as a suitable substitute for Pt in facilitating Co reduction. Moreover, the reduction temperature of cobalt oxide appears to decrease with increasing Ag loading, but with marginal improvements. It was, moreover, observed that there is a small peak appearing as a high temperature shoulder of the first peak in TPR profiles of 1.11%Ag, 1.66%Ag, 2.21%Ag, and 2.76%Ag-25%Co/Al_2O_3 catalysts. Peak area was again used for peak identification. As a result, this peak is more likely to be CoO, a fraction of which is larger and in weaker interaction with the support.

Table 7.1 The results of BET surface area and porosity measurements, hydrogen chemisorption/pulse reoxidation, and X-ray diffraction of catalysts

Catalyst	BET SA, m^2/g	Pore vol. (single point, cm^3/g	Avg pore rad., nm	H_2 desorbed per g_{cat}, μmol/g	Uncorr Metal disp., %	Uncorr Co disp.[a], %	Uncorr avg. Co^0 diam.[a], nm	O_2 uptake per g_{cat}, μmol/g	O_2 uptake by Co per g_{cat}[b], μmol/g	% Red. of Co	Corr metal disp., %	Corr Co disp.[c], %	Corr avg. Co^0 diam.[c], nm	Est. Co^0 diam from XRD[c], nm
25%Co/Al_2O_3	98.4	0.234	4.5	53.6	2.5	2.5	40.8	1008	1008	35.6	7.1	7.1	14.6	10.4
Pt promoted 25%Co/Al_2O_3														
0.5%Pt-25%Co/Al_2O_3	98.5	0.218	4.4	132.9	6.2	6.3	16.5	1759	1733	61.3	10.1	10.3	10.0	10.4
1.0%Pt-25%Co/Al_2O_3	103.9	0.255	4.9	157.6	7.3	7.4	13.9	1856	1805	63.8	11.4	11.7	8.8	8.8
2.0%Pt-25%Co/Al_2O_3	108.8	0.229	4.2	151.2	7.0	7.1	14.4	1699	1596	56.4	12.1	12.8	8.1[d]	9.7
3.0%Pt-25%Co/Al_2O_3	111.9	0.226	4.2	172.2	7.8	8.1	12.7	1799	1646	58.2	13.1	13.9	7.4[d]	8.4
4.0%Pt-25%Co/Al_2O_3	113.6	0.237	4.2	163.5	7.4	7.7	13.5	1719	1514	53.5	13.2	14.3	7.2[d]	8.6
5.0%Pt-25%Co/Al_2O_3	123.4	0.228	3.7	185.1	8.4	8.7	11.8	1758	1502	53.1	15.0	16.4	6.3[d]	8.6
Ag promoted 25%Co/Al_2O_3														
0.276%Ag-25%Co/Al_2O_3	95.5	0.224	4.7	113.0	5.3	5.3	19.3	1688	1688	59.7	8.6	8.9	11.5	9.2
0.553%Ag-25%Co/Al_2O_3	101.4	0.237	4.7	109.1	5.1	5.1	20.1	1784	1784	63.1	7.7	8.2	12.7	9.6
1.11%Ag-25%Co/Al_2O_3	102.1	0.245	4.8	108.4	5.0	5.1	20.2	1717	1717	60.7	8.2	8.4	12.3	10.0
1.66%Ag-25%Co/Al_2O_3	100.5	0.245	4.9	97.8	4.5	4.6	22.4	1700	1700	60.1	6.9	7.7	13.5	10.1
2.21%Ag-25%Co/Al_2O_3	97.3	0.236	4.9	90.3	4.1	4.3	24.2	1748	1748	61.8	6.5	6.9	15.0	9.2
2.76%Ag-25%Co/Al_2O_3	95.6	0.222	4.7	100.7	4.5	4.8	21.7	1729	1729	61.1	7.0	7.8	13.3	9.8

[a]Assume H_2 desorbed from only Co metal sites.

[b]Assume oxidation of Pt^0 to PtO_2 (Rehr et al., 1992) and no oxidation of Ag^0 (Weaver et al., 2005).

[c]From analysis of 2θ peak at 37° for Co_3O_4 (3 1 1) and assuming a contraction of 0.75 in converting to the metal after reduction.

[d]Assumption that H_2 desorbed only from Co metal sites slightly underestimates Co^0 size at higher promoter loadings.

The justification for this is that the area of this peak combined with that of the broad high temperature peak is approximately 3 times that of the first peak. It is widely suggested that H_2 dissociation and spillover on the Pt metal surface is likely to be a catalytic mechanism for accelerating cobalt oxide reduction (Jacobs et al., 2002; Jacobs et al., 2007; Jacobs et al., 2009; Wang et al., 1991), even though the precise mechanism still remains unclear. However, EXAFS results from our previous work (Jacobs et al., 2004) and of (Guczi et al., 2002) have reported that platinum is in contact with cobalt at the atomic level, forming Pt-Co bonds, and therefore a chemical effect (i.e., alloy as an active phase) should also be considered. The promotion of Ag in Co/Al_2O_3 catalyst was also reported in our previous work (Jacobs et al., 2009), and a preliminary XAS study showed that highly dispersed silver oxide particles were present and likely to be in close proximity to cobalt oxide in freshly calcined catalysts. After reduction, the Ag metal phase was detected at high Ag loading. Therefore, it is reasonable to suggest H_2 dissociation and spillover on the Ag metal surface as a possible mechanism. It is important to determine if Ag-Co bonds are detected at lower Ag loadings.

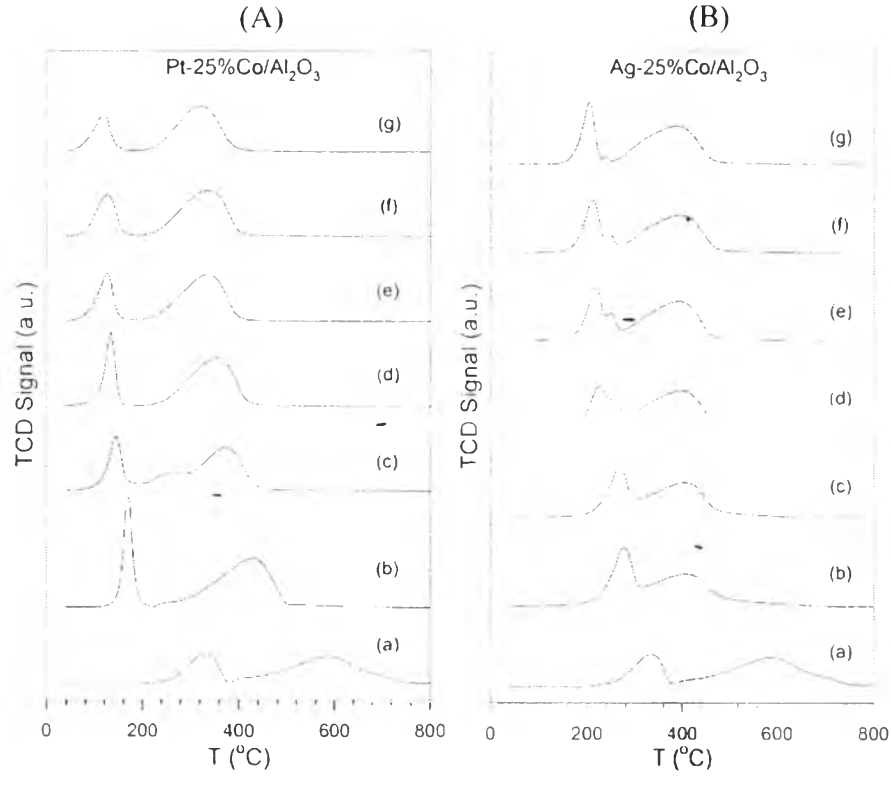

Figure 7.1 (A) TPR profiles of (a) unpromoted and Pt promoted 25%Co/Al_2O_3 catalysts, including (b) 0.5%, (c) 1.0%, (d) 2.0%, (e) 3.0%, (f) 4.0%, and (g) 5.0% by weight Pt. (B) TPR profiles of (a) unpromoted and Ag promoted 25%Co/Al_2O_3 catalysts, including (b) 0.276%, (c) 0.553%, (d) 1.11%, (e) 1.66%, (f) 2.21%, and (g) 2.76% by weight Ag, atomically equivalent to those of Pt, respectively.

7.4.3 Hydrogen Chemisorption/Pulse Reoxidation and X-ray Diffraction

Evidence from TPR profiles illustrates that adding either Pt or Ag does lead to a substantial improvement in the reduction of cobalt oxides in Co/Al_2O_3 catalysts and, moreover, the type of metal promoter (i.e., Pt or Ag) and their loadings appear to exhibit significant differences in reducing cobalt oxides. To verify whether those improvements translate into improved Co metal site densities and how well Pt or Ag facilitate Co oxide reduction as a function of loading, H_2 chemisorption and pulse reoxidation were utilized. Chemisorption of hydrogen following reduction in hydrogen at 350 °C for 10 h at atmospheric pressure was utilized to obtain the

number of metal surface atoms, which is calculated by the amount of H_2 desorbed from TPD analysis (Jacobs et al., 2002). It was found that with Pt the number of metal sites more than doubled compared to the unpromoted catalyst, and metal site density also increased with increasing Pt loading. For Ag promoter, metal site density also increased but approximately doubled and appeared to decrease with further increases in Ag loading. These improvements for both Pt and Ag promoted catalysts are consistent with the temperature shifts observed in TPR in Figure 7.1 as mentioned previously. Because of the ability of Pt and Ag metal to adsorb H_2, the measurement of the actual Co^0 metal surface sites may be complicated. Thus, in this report, we represent the dispersion by 2 terms: total metal dispersion and Co^0 metal dispersion (by assuming H_2 only from Co surface). By taking into account both Co and metal promoter, the uncorrected metal dispersion (i.e., which erroneously presumes that the Co and metal promoter are completely reduced) shown in column 6 of Table 1 was increased significantly after adding promoter. Adding 5.0% Pt by weight shifts % metal dispersion to 8.36% (threefold higher than unpromoted), which is also more pronounced than at lower Pt loading. This is different from the case of Ag, where increasing Ag slightly decreases % metal dispersion relative to lower Ag loadings, while just up to around a twofold higher improved % metal dispersion from the unpromoted catalyst was observed at the lowest loading of 0.276%Ag (atomically equivalent to 0.5%Pt). By ignoring H_2 chemisorption on metallic Pt and Ag, the uncorrected Co dispersion is obtained, and uncorrected Co dispersion is slightly higher than uncorrected metal dispersion but the same trend remains. Quantifying the degree of reduction of cobalt is necessary in order to obtain the corrected metal dispersion and a more accurate estimate of Co cluster size. The oxygen pulse reoxidation experiment was immediately performed after the TPD experiment. The total oxygen consumed is directly related to total metal reduced with the assumption that Co oxidized into Co_3O_4. For metal promoted Co/Al_2O_3 catalyst, the possibility of metallic metal promoter to be simultaneously oxidized with Co metal during pulse reoxidation must be considered. Pt metal should be oxidized into PtO_2 after complete reoxidation by oxygen pulses. The previous study of the oxidation of Pt(1 1 1) by gas phase oxygen atoms by Weaver et al. (Weaver et al., 2005) suggested PtO_2 as a main platinum oxide species instead of PtO after

oxidation at 177 °C; moreover it can be thermally tolerated up to 427 °C (Weaver et al., 2005). Also, the thermal decomposition of PtO_2 ($PtO_2 \rightarrow Pt + O_2$) on carbon has been reported at 500 °C (Kinoshita, 1977), so that PtO_2 is more likely to exist after oxygen pulse reoxidation in our case. Accordingly, to correct O_2 consumption by Co metal sites, O_2 consumed by Pt ($Pt + O_2 \rightarrow PtO_2$) must be deducted. In the case of Ag, the O_2 consumed by Ag metal is negligible because of the instability of any silver oxide forms at 350 °C, at which pulse reoxidation is performed (Jacobs et al., 2009).

It is clear that addition of either Pt or Ag led to a considerable increase in the extent of reduction relative to the unpromoted catalyst (i.e., ~70% increase for either 0.5%Pt or 0.276%Ag promoted catalysts), which is consistent with the results of reduction temperature shifts to lower temperature as observed in the TPR profiles. Therefore, it should be stressed that the role of Pt and Ag promoter is not merely to improve the reducibility of cobalt oxide but primarily to augment the Co^0 active site densities, as previously demonstrated (Cook et al., 2012; Guczi et al., 2002; Jacobs et al., 2004; Jacobs et al., 2002; Jacobs et al., 2007; Jacobs et al., 2009). Considering the effect of Pt loading, it appears that increasing Pt slightly decreases %Co reduction at high loading, as estimated by O_2 titration, and this is consistent with TPR. This in turn impacts the corrected average Co cluster size, which appears to become smaller as Pt loading increases. It is suggested that higher Pt contents lead to a greater fraction of smaller cobalt oxide clusters being reduced, thereby resulting in an increase in the fraction of smaller Co clusters. The trend of Co cluster size versus Pt loading is further supported by the size estimated by X-ray diffraction (i.e., the Co crystal size of Co_3O_4 at $2\theta = 37°$ after applying a contraction factor of 0.75).

XRD diffraction profiles of Pt-25%Co/Al_2O_3 and Ag-25%Co/Al_2O_3 catalysts are shown in Figure 7.2(A) and Figure 7.2(B), respectively. Results of line broadening analysis for evaluating Co metal size (i.e., the Co crystal size of Co_3O_4 at $2\theta = 37°$ and applying a contraction factor of 0.75) in each catalyst are summarized in the last column of Table 7.1. XRD results show that in all cases, the estimated Co^0 size is similar. Interestingly, while at low loadings of either Ag or Pt, the chemisorption results are close to the estimates from XRD, at higher loadings of Pt there is a deviation toward slightly smaller size, and with Ag there is a deviation

toward slightly larger size. The latter may in part reflect a diffusion problem of O_2 penetrating the core of larger metal particles (Hilmen et al., 1996). As we will show from reaction testing data, the deviations are likely due not to a real change in actual cluster size, but rather to promoter location. With Pt, it appears that there may be a fraction of Pt exposed on the surface and contributing to the H_2-TPD. With Ag, there is likely a fraction that essentially blocks Co surface sites, resulting in a slight attenuation of the Co site density. While an increase in BET surface area and a decrease in average pore radius after increasing Pt loading suggest that at the higher Pt loadings, a fraction of Pt resides on the support, because no Pt-Pt bonds are observed in EXAFS (to be discussed) suggests that the Pt is incorporated with Co^0 clusters during reduction. For Ag promoter, the agglomeration of Ag to form larger Ag clusters during reduction at 350 °C was proposed in our previous report (Jacobs et al., 2009). Thus, the possibility of some pore blocking at high Ag loading following activation should be considered. Note that there was no significant change in BET results even at high Ag loadings after calcination, implying that the Ag is, prior to reduction, well dispersed on the surface of Co/Al_2O_3 catalyst as small Ag_2O clusters (Jacobs et al., 2009; Kuzmin et al., 2006). The Ag_2O clusters formed after calcination are likely located near Co_3O_4 to play a pivotal role in facilitating cobalt oxide reduction as described above. According to this point, the possibility of Ag-Co formation was postulated and investigated by XAS study in this study. In conclusion, although Ag promoter is able to satisfactorily promote Co reduction, it may be unable to provide similar Co site densities as observed with Pt promoter. However its promoting ability and lower cost make it alluring as a possible alternative promoter.

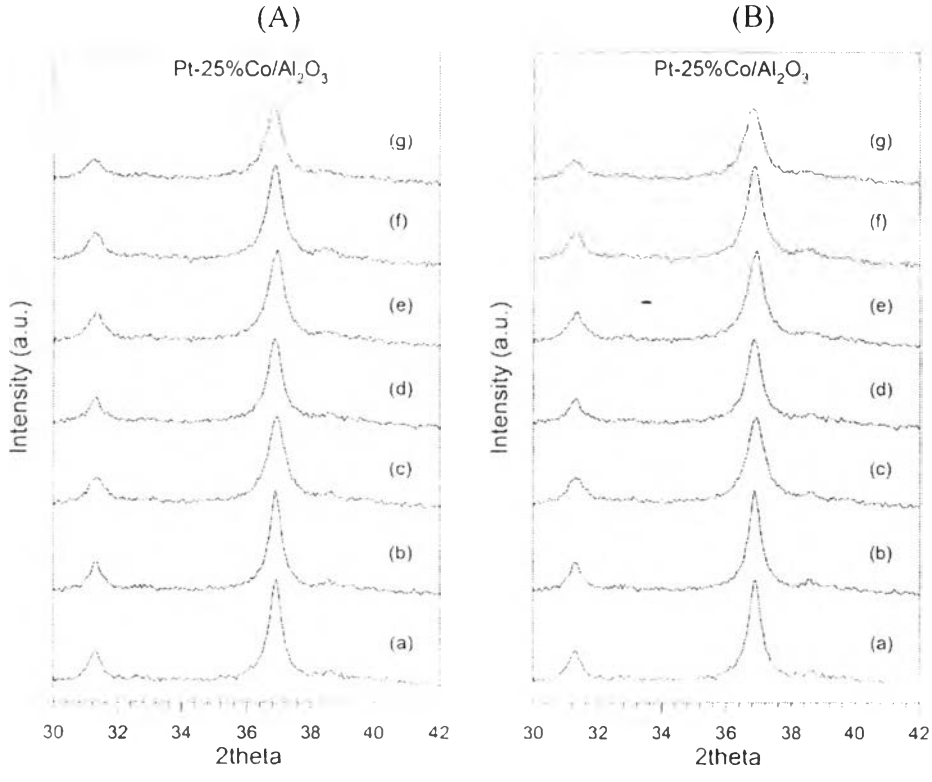

Figure 7.2 (A) X-ray diffraction profiles of (a) unpromoted and Pt promoted 25%Co/Al_2O_3 catalysts, including (b) 0.5%, (c) 1.0%, (d) 2.0%, (e) 3.0%, (f) 4.0%, and (g) 5.0% by weight Pt. (B) X-ray diffraction profiles of (a) unpromoted and Ag promoted 25%Co/Al_2O_3 catalysts, including (b) 0.276%, (c) 0.553%, (d) 1.11%, (e) 1.66%, (f) 2.21%, and (g) 2.76% by weight Ag, atomically equivalent to those of Pt, respectively.

7.4.4 XANES and EXAFS Spectroscopies

The normalized XANES spectra measured at the Pt L_{III}-edge in Figure 7.3(A) consist of two spectra of the 0.5%Pt-25%Co/Al_2O_3 catalysts: the one calcined (350 °C, in air flow, 4 h) and the other reduced (350 °C, in 4%H_2/He flow, 10 h), Pt metal, and two platinum oxides: PtO and PtO_2. The Pt L_{III} absorption edge at ~11.566 keV of the calcined catalyst is close to that of PtO_2, which absorbs at 11.566 keV edge (i.e., +2 eV shift from E_0 of 11.564) (Christensen et al., 2009). By comparing the XANES region (i.e., $E_0 - 100$ eV < E < $E_0 + 40$ eV; $E_0 = 11.564$ keV),

the XANES line shapes of calcined Pt-25%Co/Al_2O_3 and PtO_2 are also similar. Moreover, the white intensity of calcined catalyst more closely resembles to that of PtO_2 rather than PtO. The white line intensity in this case for platinum is related to the d-electron density of states. An increase in the white line intensity directly shows a decrease in the number of electrons in the d orbital, such that the white line of PtO (Pt^{2+}) and PtO_2 (Pt^{4+}) can be distinguished. An investigation of Pt in calcined Pt/Co catalyst has also shown that Pt is in the Pt^{4+} oxidation state (Cook et al., 2012). On the other hand, after reduction PtO_2 is converted into Pt metal as evidenced by comparing the XANES spectrum to that of the Pt metal reference.

To observe the temperature-dependent changes of the oxidation state of platinum during H_2 reduction, the TPR-XANES technique was applied. TPR-XANES spectra of Pt- 25%Co/Al_2O_3 catalyst with 3 different Pt loadings are depicted in Figure 7.3(B). It is clearly seen that XANES spectra of all catalysts change significantly with increasing reduction temperature as platinum oxides are converted to metallic Pt. Platinum (II) oxide (PtO) is an intermediate Pt species, which is detectable by XANES spectra. A lower white line intensity compared to PtO_2, a higher white line intensity compared to Pt metal, and a +1 eV shift from E_0 at the Pt L_{III}–edge were evident. Thus, linear combination fittings of the XANES spectra of the catalyst samples were performed using PtO_2, PtO, and Pt metal XANES spectra and the fitting results are shown on the right side of Figure 7.3(B). It was found that Pt loading has a measurable effect on its reducibility. Increasing Pt noticeably decreases the reduction temperature of PtO_2 and PtO respectively, thereby allowing the Pt metal to form at lower temperature. 18%PtO was found in 5.0%Pt-25%Co/Al_2O_3 catalyst, even at the temperature of reduction as low as 50 °C. The maximum content of PtO in each catalyst sample was found at different temperatures, namely, 185 °C, 150 °C, and 125 °C for 0.5%Pt, 2.0%Pt, and 5.0%Pt-25%Co/Al_2O_3, respectively. The onset temperature of Pt metal formation was also found to decrease with increasing loading (210°C, 175 °C, and 125 °C were observed at 0.5%Pt, 2.0%Pt, and 5.0%Pt-25%Co/Al_2O_3, respectively). However, platinum oxides in all catalysts were successfully reduced into Pt metal at 350 °C, as also shown in Figure 7.3(C). In conclusion, the rate of platinum oxide conversion to Pt metal is improved by adding more platinum. It has been suggested that a

nucleation/growth model may dominate this reduction process. That is, once Pt metal nuclei have formed, they serve to facilitate other nearby metal oxides to be reduced, which is possibly by a H_2 dissociation and spillover mechanism; moreover, increasing Pt loading, while it is costly to do so, accelerates this process. Pt metal formed during the reduction process facilitates not merely further platinum oxide reduction but cobalt oxide reduction as well, as the reduction temperatures of cobalt oxides were obviously shifted to lower temperature for Pt-25%Co/Al_2O_3 catalyst as shown in Figure 7.1(A).

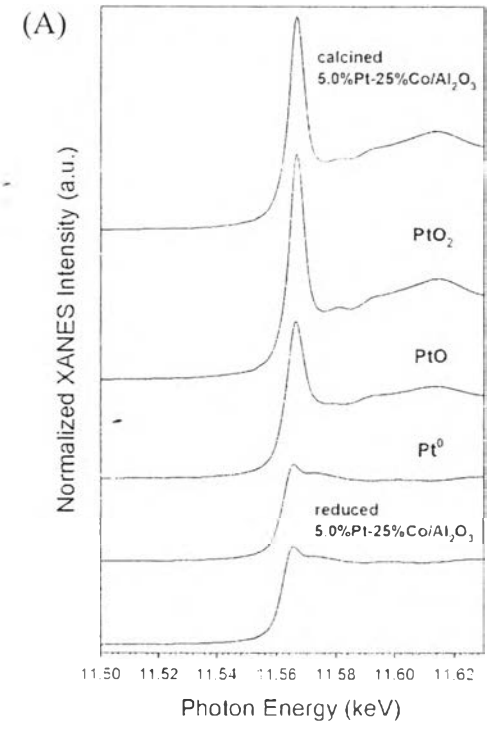

(B)

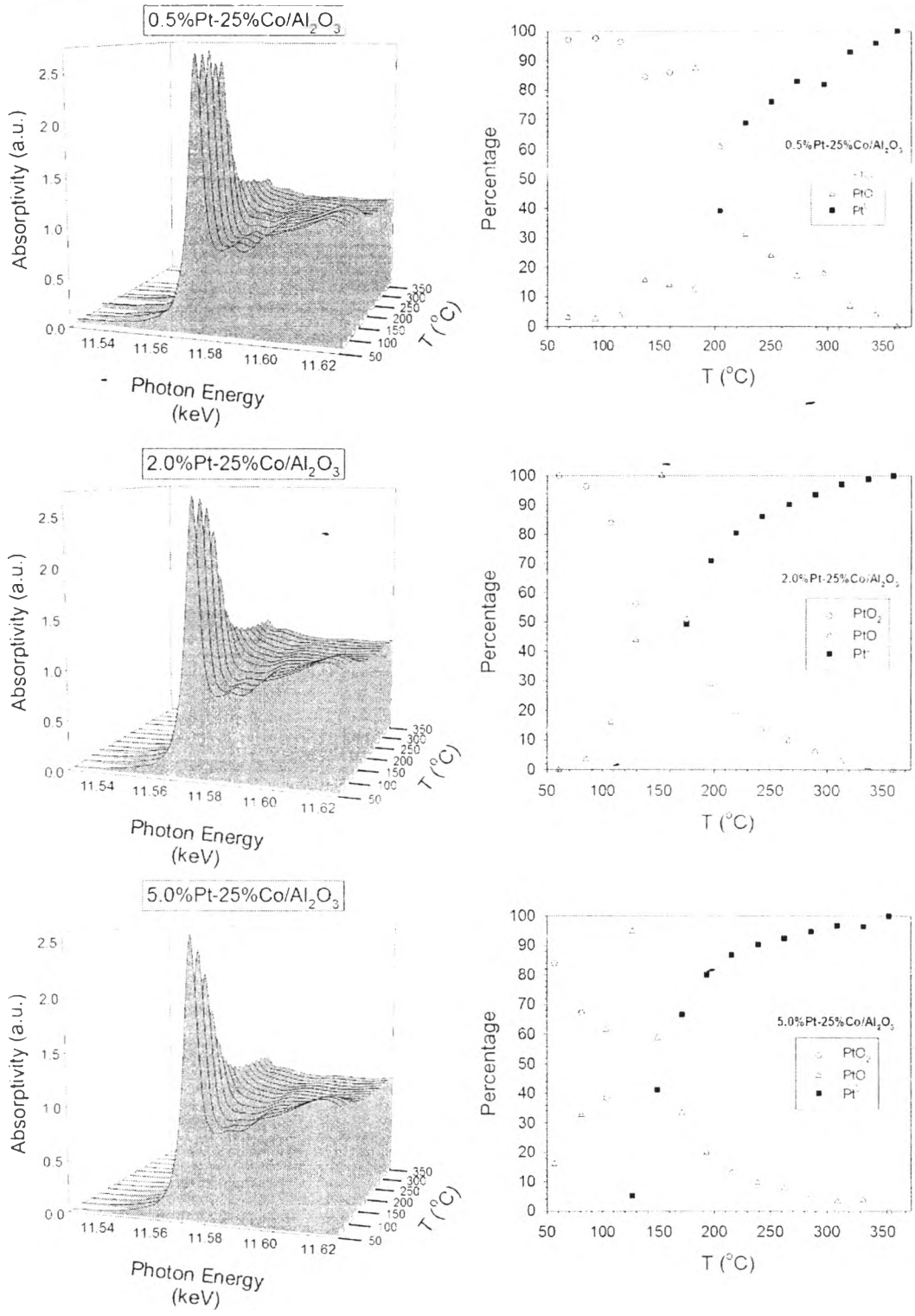
0.5%Pt-25%Co/Al2O3
Absorptivity (a.u.)
Photon Energy (keV)
T (°C)
Percentage
PtO2
PtO
Pt
2.0%Pt-25%Co/Al2O3
5.0%Pt-25%Co/Al2O3

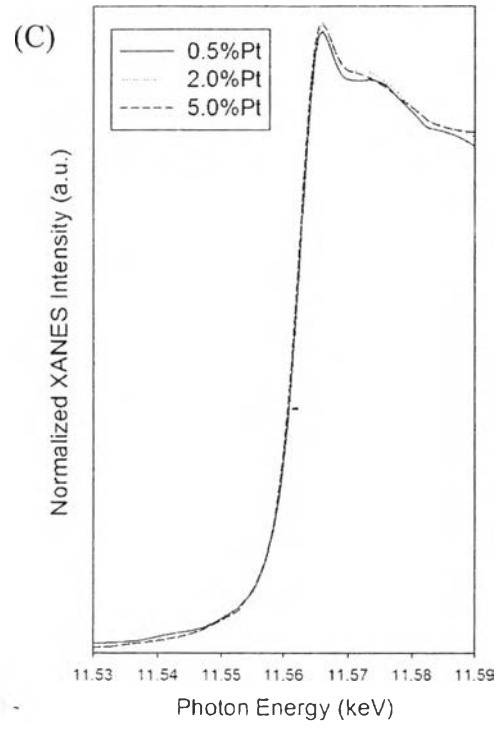

Figure 7.3 (A) Normalized XANES spectra at the Pt L_{III}-edge of Pt-25%Co/Al_2O_3 catalysts (calcined and reduced) and Pt reference compounds; PtO, PtO_2, and Pt^0. (B) (left) TPR-XANES spectra and (right) their corresponding linear combination fittings from reference spectra in Figure 7.3 (A) of, moving down, 0.5%Pt-25%Co/Al_2O_3; 2.0%Pt-25%Co/Al_2O_3; and 5.0%Pt-25%Co/Al_2O_3. (C) Normalized XANES spectra at the Pt L_{III}-edge of Pt promoted Co/Al_2O_3 catalysts with different loadings; (solid line) 0.5%Pt, (dotted line) 2.0%Pt, and (dashed line) 5.0%Pt, after TPR after cooling to ambient conditions.

To investigate the local atomic structure of Pt promoted Co/Al_2O_3 catalysts, EXAFS analysis was performed. Figure 7.4(A) provides the k^3-weighted EXAFS Fourier Transform magnitude spectra of the Pt L_{III}-edge for relevant platinum reference compounds (i.e., Pt^0 and PtO_2) for calcined and reduced catalysts. The FT magnitude spectrum of the calcined catalyst is comprised of peaks for Pt-O and Pt-Pt coordination. The spectra differed from bulk PtO_2, as the peaks representing the first shell coordination of Pt-O and Pt-Pt are both shifted to lower

distance compared to the bulk PtO_2, possibly due to the contraction of those bonds for small platinum oxide particles. After reduction, the reduced catalyst showed a distinct peak at about 2.1 Å in the phase-uncorrected spectra. This peak position is not the first coordination shell of Pt metal, which is located at around 2.7 Å in the phase uncorrected spectra. The change in Pt coordination environment with the reduction temperature can be observed in TPR-EXAFS spectra in Figure 7.4(B). A low temperature Pt coordinates with both oxygen and platinum atoms as Pt is in the form of PtO_2; then, at around 175 °C those bonds decrease, while a distinct peak (~ 2.1 Å) starts to form and becomes more obvious as the reduction temperature increases. As Pt atom was the core atom, the change in the position of the FT magnitude of Pt-Pt bond (~0.6 Å shift to closer) indicates that Pt-Pt bonds were not detected after reduction but, rather, Pt-Co bonds were formed (Cook et al., 2012; Guczi et al., 2002; Jacobs et al., 2004). Though Pt-Co bond formation has been explored, the effect of Pt loading on the formation of this bimetallic bond has not been disclosed. The results of the modeling procedure using FEFFIT for the k^3-weighted EXAFS Fourier Transform magnitude spectra and filtered k^3-weighted $\chi(k)$ spectra of Pt-promoted catalyst following TPR experiment and cooling to ambient conditions are shown in Figure 7.4(C). The well-defined peak corresponds to Pt-Co bonding (Guczi et al., 2002; Jacobs et al., 2004). The solid lines in Figure 7.4(C) show the experimental data, while the circles provide the best fit. The fitting parameters are summarized in Table 7.2. Generally, the r-factor value of <0.02 indicates a good fit, and all catalyst spectra fall below this value. The results suggest that the majority of Pt is in intimate contact with the cobalt cluster. The preference of Pt to form bonds with Co is also stressed by results of varying Pt loading, even when high amounts of Pt are applied. Moreover, increasing Pt does not have a significant effect on Pt-Co coordination number among reduced catalysts with different Pt loading, as the numerical results of Pt-Co coordination number with a wide range of deviation are shown in column 2 of Table 7.2. Although Figure 7.4(D), an overlaid graph depicting a comparison of Pt-Co peak intensity of all catalysts after reduction, provides an easily observed difference in intensity, it is not statistically different as mentioned above. Thus, it is suggested that even at high Pt loading, Pt^0 still remains in good contact with Co^0. However, the degree of

coordination between Pt and Co is expected at the lowest Pt loading, at which lowest molar ratio of Pt to Co is present. While the authors are fully aware that high costs already preclude the use of Pt at high loadings, the loading study serves as a point of reference for comparing potentially less expensive promoters, where higher promoter loadings may be acceptable.

Investigating silver promoter in Ag promoted Co/Al_2O_3 catalyst, XAS scanning at the Ag K-edge energy was performed for both relevant Ag reference compounds and catalysts (before and after reduction). As a result, the XANES spectra and the local atomic structure of Ag in this catalyst were revealed in this work. As shown in Figure 7.5(A), Ag in the calcined $Ag\text{-}25\%Co/Al_2O_3$ catalyst did not resemble either bulk Ag_2O or bulk AgO references. Referring to results from previous work (Kuzmin et al., 2006), which investigated $Ag_2O\text{-}B_2O_3$ mixed oxides and with our previous report (Jacobs et al., 2009), the spectrum representing the calcined catalyst is likely indicative of highly dispersed Ag_2O particles located in close proximity to cobalt oxide domains. On the other hand, the spectrum of reduced $0.276\%Ag\text{-}25\%Co/Al_2O_3$ matches that of the Ag foil. Moreover, due to the higher FT magnitude observed for the Ag foil relative to the reduced catalyst, it can be implied that the Ag-Ag coordination number in the reduced catalyst is not as large as that of the Ag foil (i.e., with FCC structure and first shell coordination number of 12). To observe electronic changes of Ag during the reduction process, a TPR-XANES experiment was conducted and the resulting spectra of catalysts with 3 different Ag loadings are depicted in Figure 7.5(B). In Figure 7.5(B) (left), the white line intensity decreased with increasing reduction temperature, indicating a gradual change from silver oxide to Ag metal.

(A)

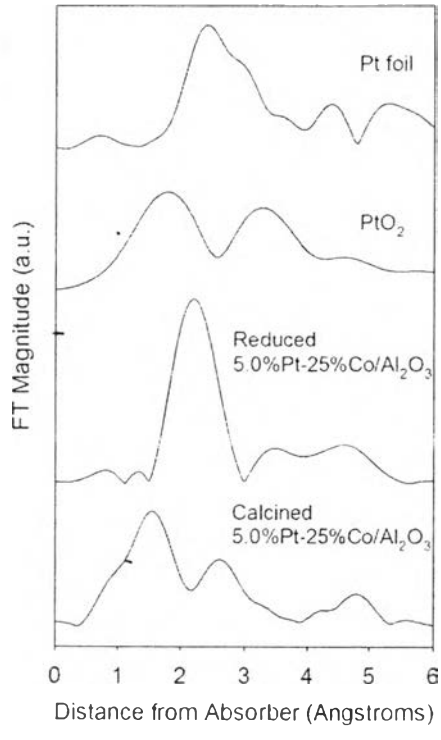
Pt foil
PtO2
Reduced
5.0%Pt-25%Co/Al2O3
Calcined
5.0%Pt-25%Co/Al2O3
FT Magnitude (a.u.)
0 1 2 3 4 5 6
Distance from Absorber (Angstroms)

(B)

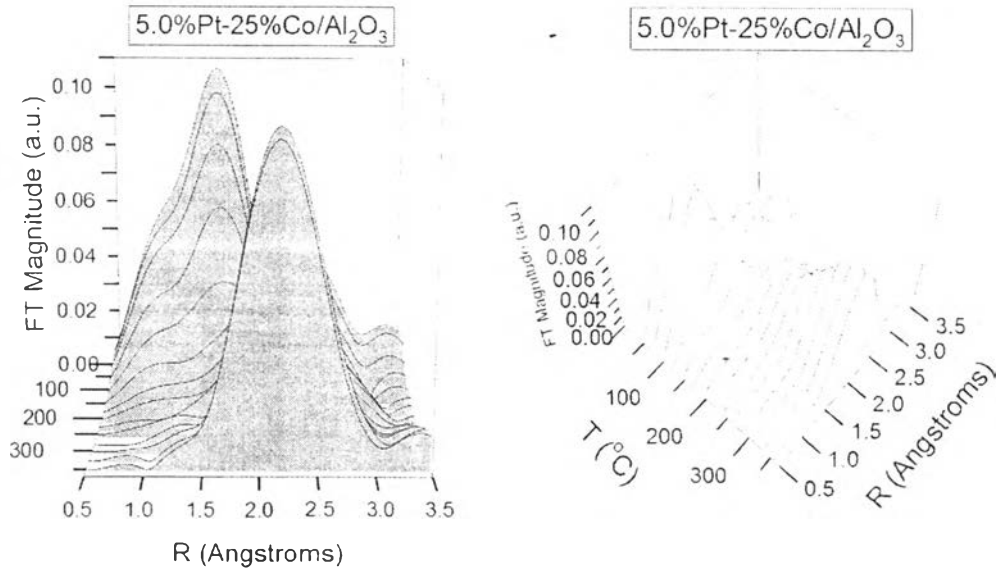
5.0%Pt-25%Co/Al2O3
FT Magnitude (a.u.)
0.10
0.08
0.06
0.04
0.02
0.00
100
200
300
0.5 1.0 1.5 2.0 2.5 3.0 3.5
R (Angstroms)
5.0%Pt-25%Co/Al2O3
T (°C)
R (Angstroms)

(C)

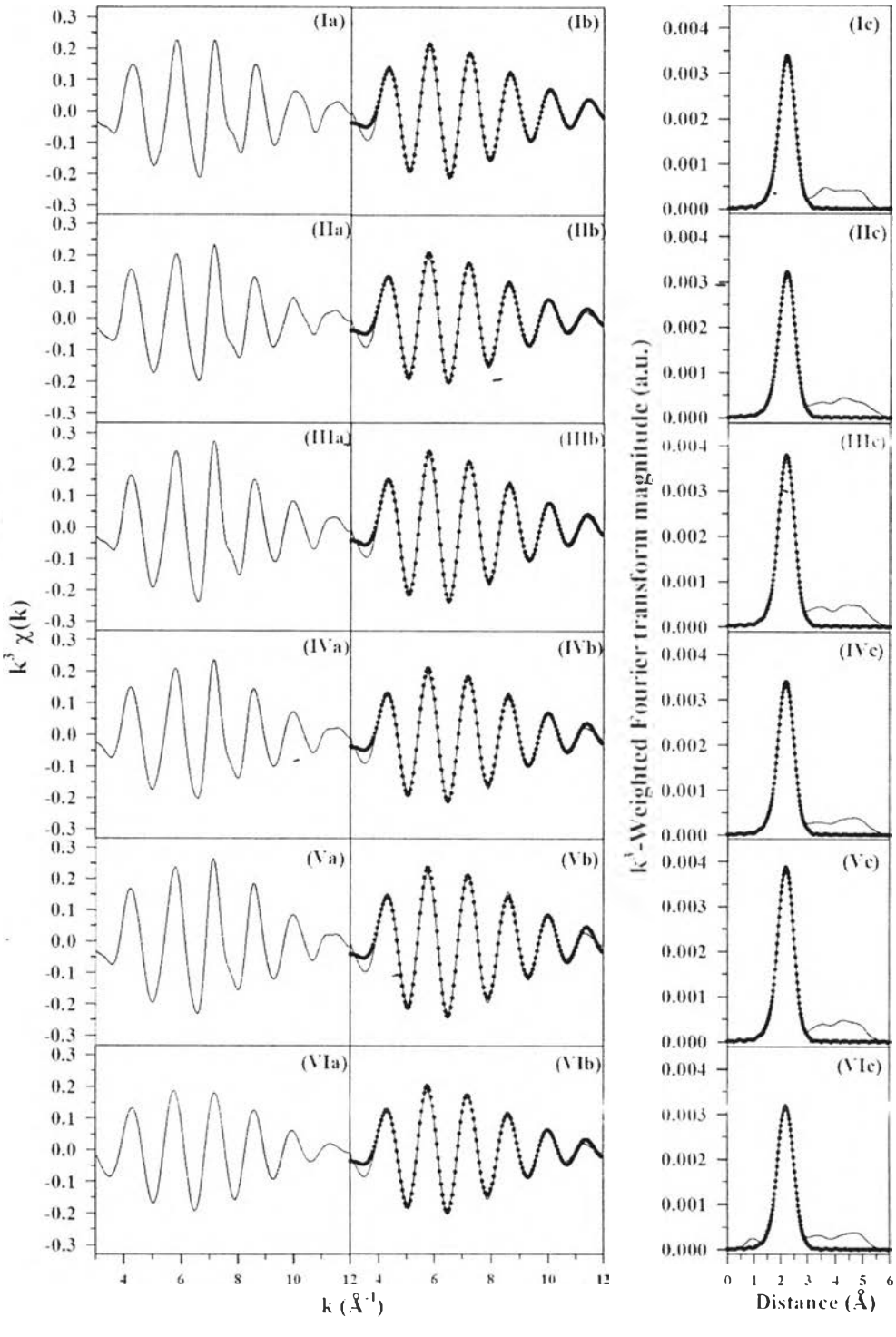
(Ia)
(Ib)
(Ic)
(IIa)
(IIb)
(IIc)
(IIIa)
(IIIb)
(IIIc)
(IVa)
(IVb)
(IVc)
(Va)
(Vb)
(Vc)
(VIa)
(VIb)
(VIc)
k³ χ(k)
k (Å⁻¹)
k³-Weighted Fourier transform magnitude (a.u.)
Distance (Å)

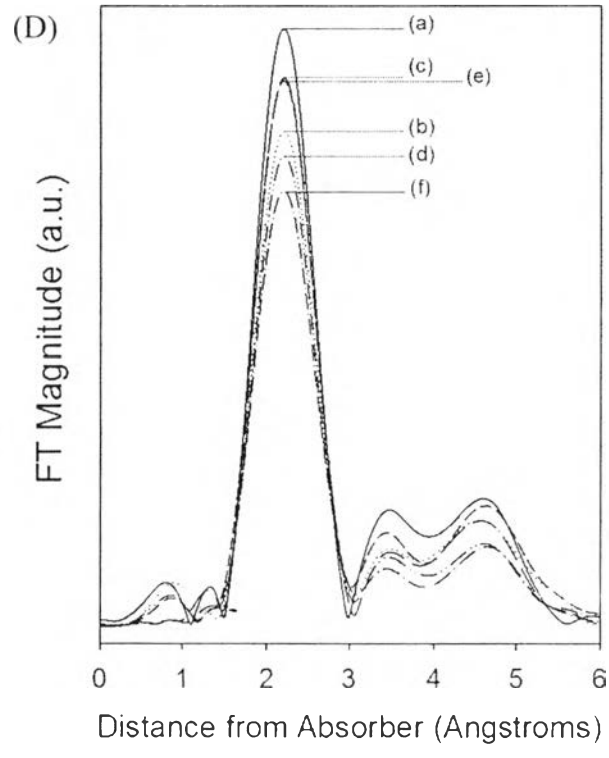

Figure 7.4 (A) k^3-Weighted EXAFS Fourier transform magnitude spectra of Pt promoted Co/Al_2O_3 catalysts and Pt reference compounds. (B) TPR-EXAFS k^3-Weighted Fourier transform magnitude spectra of 5.0%Pt-25%Co/Al_2O_3. (C) k^3-weighted EXAFS Fourier transform magnitude spectra of Pt-promoted catalysts after TPR after cooling to ambient conditions: (a) raw $k^3 \cdot \chi(k)$ vs. k data; (b) filtered $k^3 \cdot \chi(k)$ vs. k data (solid line) and resulting fitting (filled circles); (c) Fourier transform magnitude spectra (solid line), and first shell fitting (filled), moving downward. (I) 0.5%Pt-25%Co/Al_2O_3; (II)1.0%Pt-25%Co/Al_2O_3; (III) 2.0%Pt-25%Co/Al_2O_3; (IV) 3.0%Pt-25%Co/Al_2O_3; (V) 4.0%Pt-25%Co/Al_2O_3; (VI) 5.0%Pt-25%Co/Al_2O_3. (D) k^3-Weighted Fourier transform magnitude spectra after the TPR after the catalysts were cooled to ambient conditions, (a) 0.5%Pt-25%Co/Al_2O_3; (b) 1.0%Pt-25%Co/Al_2O_3; (c) 2.0%Pt-25%Co/Al_2O_3; (d) 3.0%Pt-25%Co/Al_2O_3; (e) 4.0%Pt-25%Co/Al_2O_3; (f) 5.0%Pt-25%Co/Al_2O_3.

Table 7.2 Results of EXAFS fitting parameters for references acquired near the Pt L_{III}-edge. The fitting ranges were approximately Δk = 3-12 $Å^{-1}$ and ΔR = 1.6-2.83 Å, S_0^2 = 0.9

Catalyst	N Pt-Co	R Pt-Co (Å)	e_0 (eV)	σ^2 ($Å^2$)	r-factor
0.5%Pt-25%Co/Al_2O_3	6.6 (0.59)	2.549 (0.007)	6.00 (1.02)	0.0068 (0.00087)	0.0060
1.0%Pt-25%Co/Al_2O_3	7.0 (0.67)	2.558 (0.008)	5.99 (1.09)	0.0076 (0.00097)	0.0067
2.0%Pt-25%Co/Al_2O_3	7.6 (0.61)	2.555 (0.006)	6.18 (0.915)	0.0069 (0.00079)	0.0048
3.0%Pt-25%Co/Al_2O_3	6.7 (0.61)	2.557 (0.007)	5.64 (1.05)	0.0067 (0.00090)	0.0064
4.0%Pt-25%Co/Al_2O_3	7.2 (0.67)	2.557 (0.007)	5.83 (1.06)	0.0062 (0.00088)	0.0065
5.0%Pt-25%Co/Al_2O_3	6.6 (0.63)	2.560 (0.008)	5.54 (1.08)	0.0072 (0.00094)	0.0067

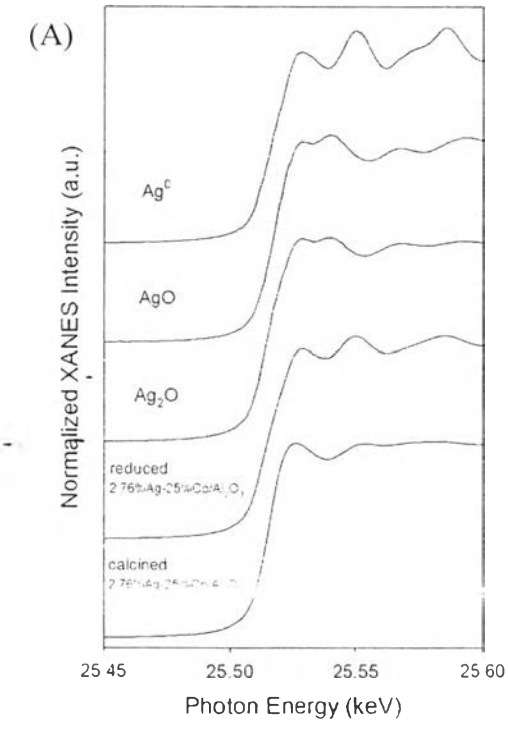

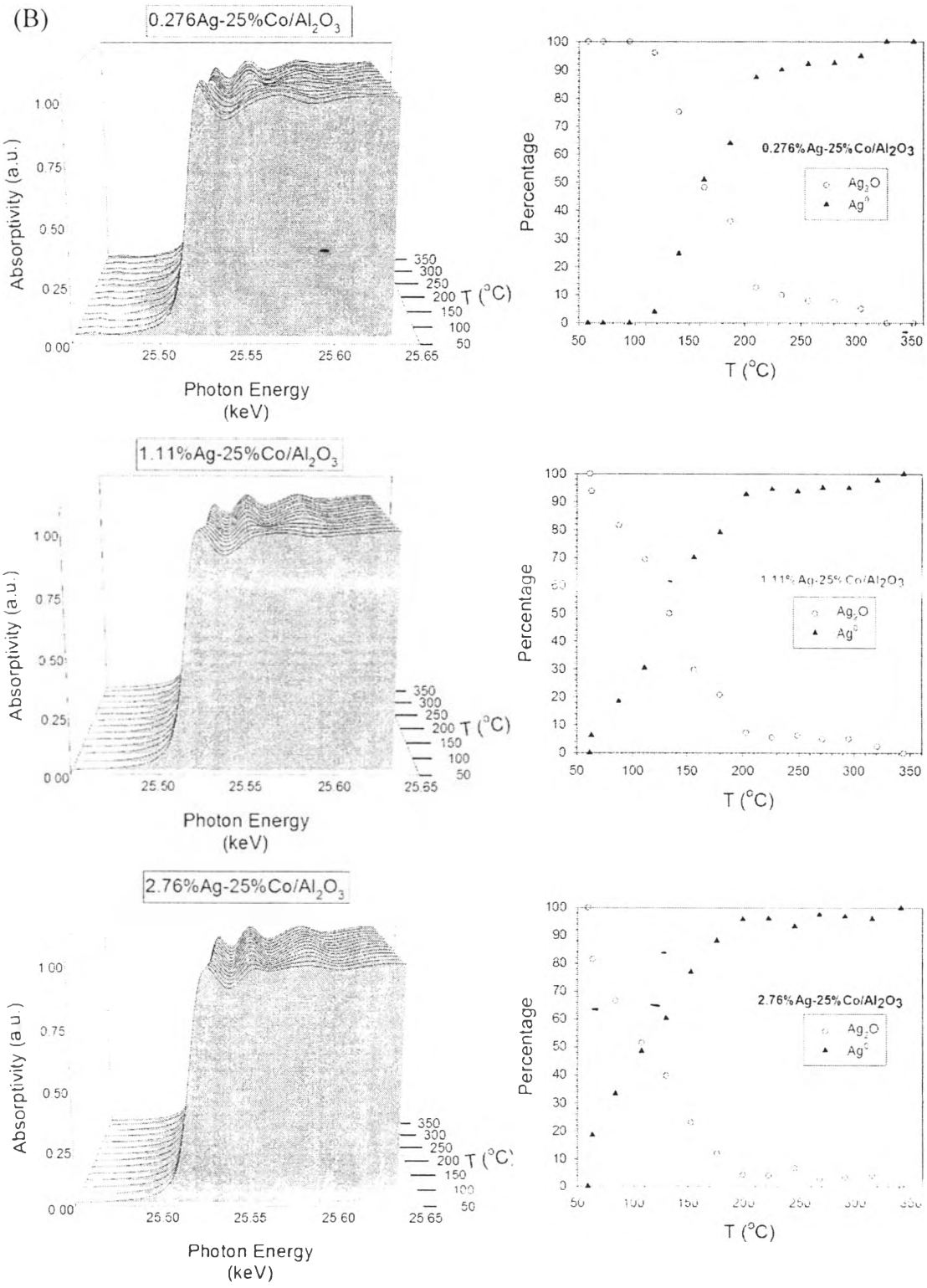
(B)
0.276Ag-25%Co/Al2O3
Absorptivity (a.u.)
Photon Energy (keV)
T (°C)
Percentage
0.276%Ag-25%Co/Al2O3
Ag2O
Ag0
1.11%Ag-25%Co/Al2O3
2.76%Ag-25%Co/Al2O3

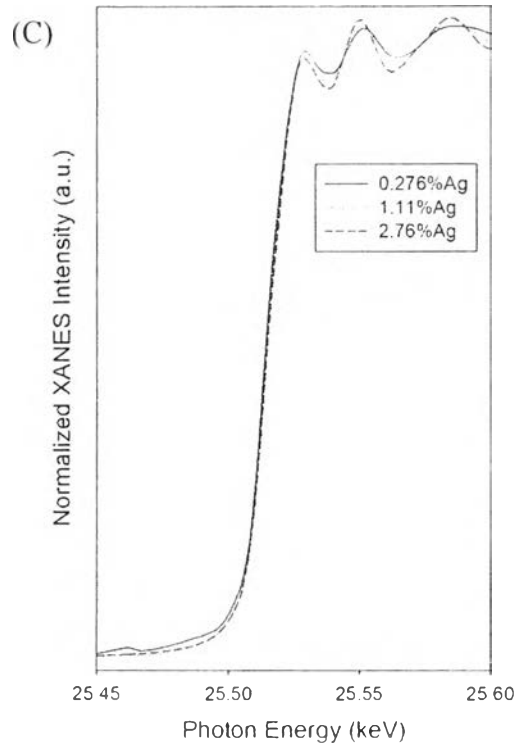

Figure 7.5 (A) Normalized XANES spectra at the Ag K-edge of Ag-25%Co/Al_2O_3 catalysts (calcined and reduced) and Ag reference compounds; AgO, Ag_2O, and Ag^0. (B) (left) TPR-XANES spectra and (right) their corresponding linear combination fittings from reference spectra in Figure 7.5 (A) of, moving down, 0.276%Ag-25%Co/Al_2O_3; 1.11%Ag-25%Co/Al_2O_3; and 2.76%Ag-25%Co/Al_2O_3. (C) Normalized XANES spectra at the Ag K-edge of Ag promoted Co/Al_2O_3 catalysts with different loadings; (solid line) 0.276%Ag, (dotted line) 1.11%Ag, and (dashed line) 2.76%Ag, after TPR after cooling to ambient conditions.

A linear combination fitting of the XANES of the catalyst samples with different Ag loadings using the Ag_2O and Ag metal XANES spectra leads to the results in Figure 7.5(B) (right). As the amount of Ag increases, Ag metal tends to form at lower temperature. The nearly equal amount (50%-50%) of Ag_2O and Ag metal is observed at 165 °C, 130 °C, and 110 °C in 0.276%Ag, 1.11%Ag, and 2.76%Ag-25%Co/Al_2O_3 catalysts, respectively. However, silver oxide present on each catalyst is completely reduced to the metallic form of Ag after H_2 activation at 350 °C, as

shown in Figure 7.5(C). A comparison of normalized XANES spectra of Ag-promoted Co/Al_2O_3 catalysts was obtained by scanning the catalysts after TPR and cooling to ambient conditions. Thus, following activation in H_2, highly dispersed silver oxides in this catalyst are transformed to Ag metal, which further facilitates the reduction of Co_3O_4 and, subsequently, CoO species, perhaps via a H_2 dissociation and spillover mechanism (Jacobs et al., 2002; Jacobs et al., 2007).

Figure 7.6(A) shows the k^1-weighted EXAFS Fourier Transform magnitude spectra of silver reference compounds (Ag^0, Ag_2O, and AgO) and catalysts (before and after reduction). In good agreement with the interpretation of the XANES spectra, the EXAFS spectra show that neither the Ag_2O spectrum nor the AgO spectrum is identical to that of the calcined catalyst, implying that silver oxides in the calcined catalyst are in interaction with the Al_2O_3 support. After reduction, two prominent peaks were formed. By comparing with the Ag^0 foil, the one located at a distance (~2.8 Å) further from the absorbing Ag atom is assigned to Ag-Ag coordination, while the nearer peak (~2.6 Å) correlates well with Ag-Co coordination. The peak corresponding to those bond distances become more obvious with increasing degree of reduction, as shown in Figure 7.6(B). To verify those peaks, a fitting procedure using FEFFIT for the k^1-weighted EXAFS Fourier Transform magnitude spectra and filtered k^1-weighted $\chi(k)$ spectra was performed for the spectra recorded after reduction and cooling to close to ambient conditions. The results of the fitting are displayed in Figure 7.6(C) and fitting parameters are summarized in Table 7.3. The model with the best fitting was obtained when the first and the second peak in reduced catalysts were assigned to Co-Ag and Ag-Ag bonds, respectively. The first shell of Ag-Co coordination number follows the trend 0.276%Ag-25%Co/Al_2O_3 > 0.553%Ag-25%Co/Al_2O_3 = 1.11%Ag-25%Co/Al_2O_3 = 1.66%Ag-25%Co/Al_2O_3 > 2.21%Ag-25%Co/Al_2O_3 > 2.76%Ag-25%Co/Al_2O_3. On the other hand, the trend of first shell Ag-Ag coordination number is opposite, with Ag likely forming isolated particles at higher Ag loading. This is evident when the spectra are superimposed in Figure 7.6(D). Therefore, the results expand upon our previous work for Ag-Co/Al_2O_3 catalyst, and reveal that in addition to the formation of Ag-Ag bonds due to segregation of Ag during reduction (Jacobs et al., 2009), Ag-

Co bonds are indeed present, such that this bimetallic species may play a role in facilitating Co reduction, as well as impacting catalytic performance during FTS.

In conclusion, the coordination of the promoter with Co is fundamentally different, as silver offers a much lower degree of coordination to cobalt on a per atom basis relative to platinum at the same atomic ratio. Moreover, Ag-Ag first shell coordination was observed even at the lowest Ag loadings after complete activation in H_2, while Pt-Pt bonds were not apparent, even at levels as high as 5%Pt. However, either Pt or Ag promoted Co/Al_2O_3 catalysts can significantly facilitate the reduction of cobalt oxides as shown by the results of TPR and H_2 chemisorption/pulse reoxidation above. This significantly different atomic structure of Ag promoter relative to Pt, a commercial promoter, could conceivably pose problems in terms of maintaining coordination following regeneration cycles.

(A)

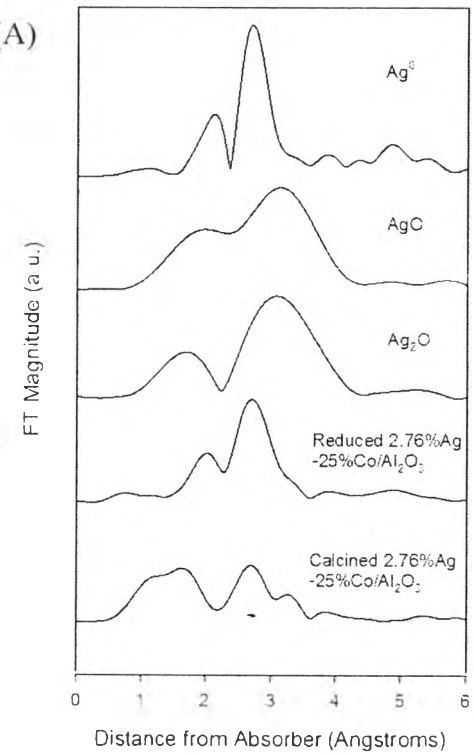
Ag°
AgC
Ag2O
Reduced 2.76%Ag -25%Co/Al2O3
Calcined 2.76%Ag -25%Co/Al2O3
FT Magnitude (a.u.)
0 1 2 3 4 5 6
Distance from Absorber (Angstroms)

(B)

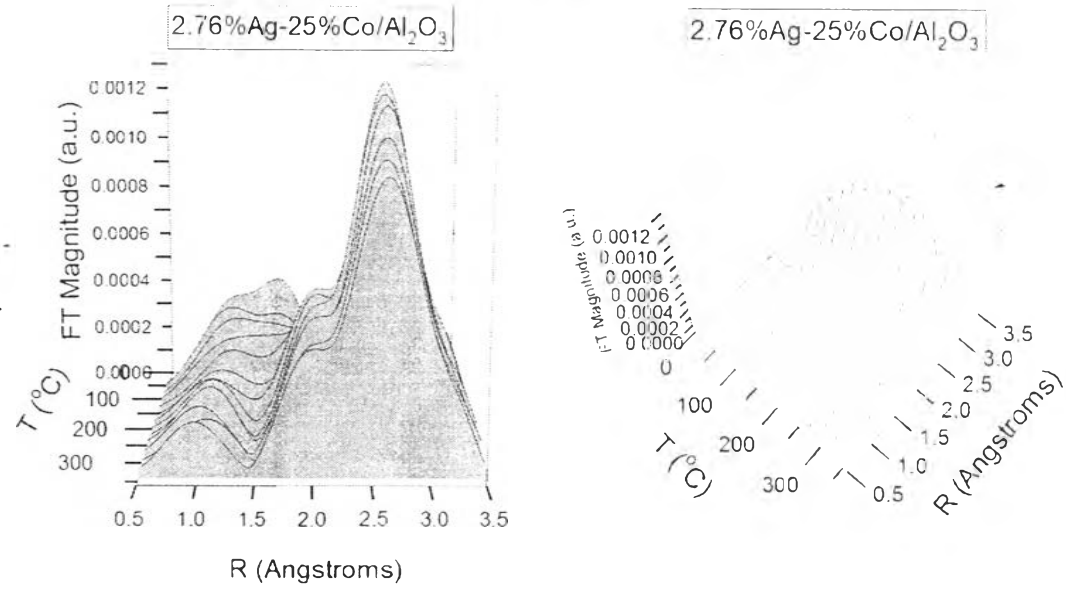
2.76%Ag-25%Co/Al2O3
FT Magnitude (a.u.)
0.0012
0.0010
0.0008
0.0006
0.0004
0.0002
0.0000
T (°C)
100
200
300
0.5 1.0 1.5 2.0 2.5 3.0 3.5
R (Angstroms)
2.76%Ag-25%Co/Al2O3
FT Magnitude (a.u.)
T (°C)
R (Angstroms)

(C)

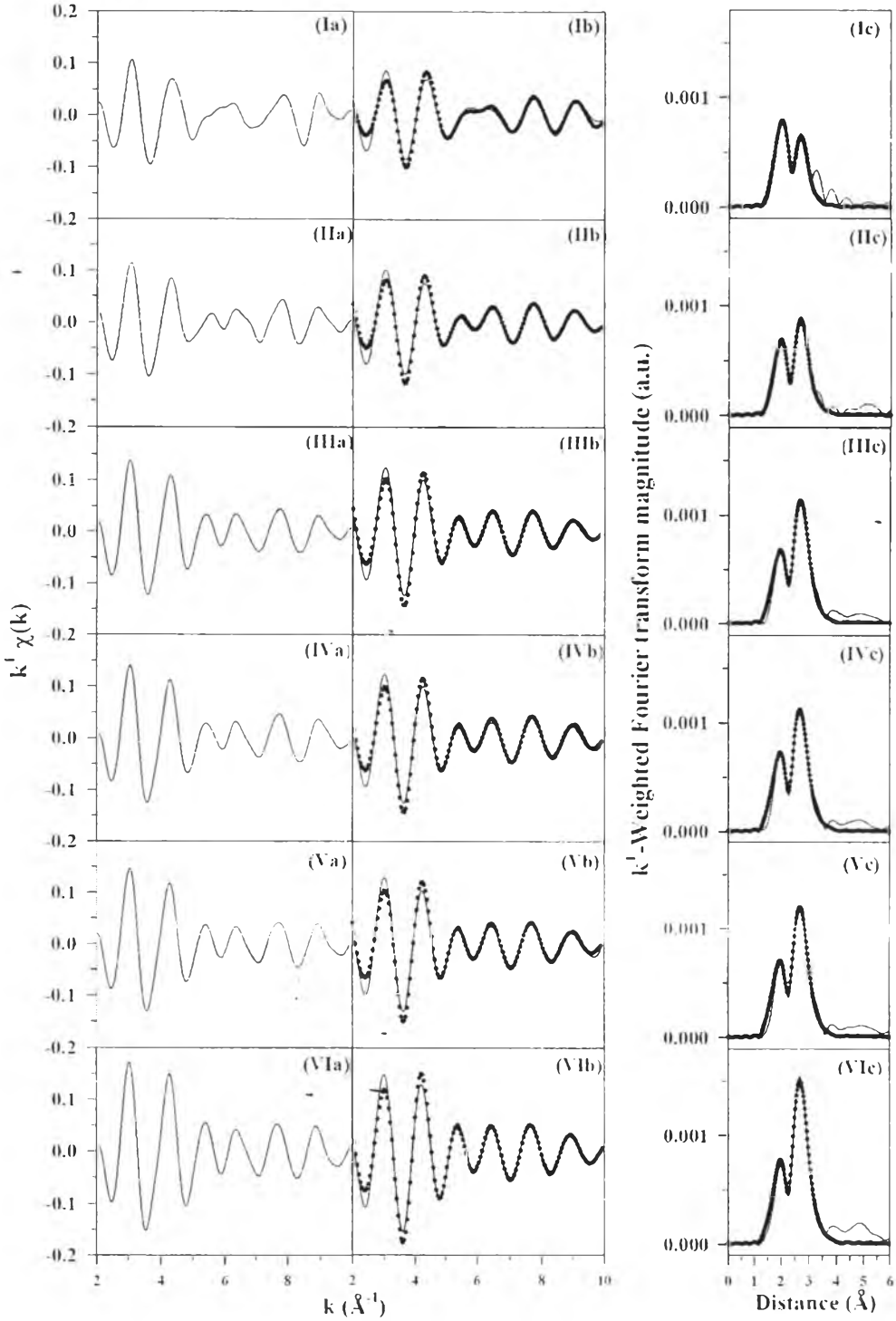
(Ia)
(Ib)
(Ic)
(IIa)
(IIb)
(IIc)
(IIIa)
(IIIb)
(IIIc)
(IVa)
(IVb)
(IVc)
(Va)
(Vb)
(Vc)
(VIa)
(VIb)
(VIc)
k¹ χ(k)
k (Å⁻¹)
k¹-Weighted Fourier transform magnitude (a.u.)
Distance (Å)

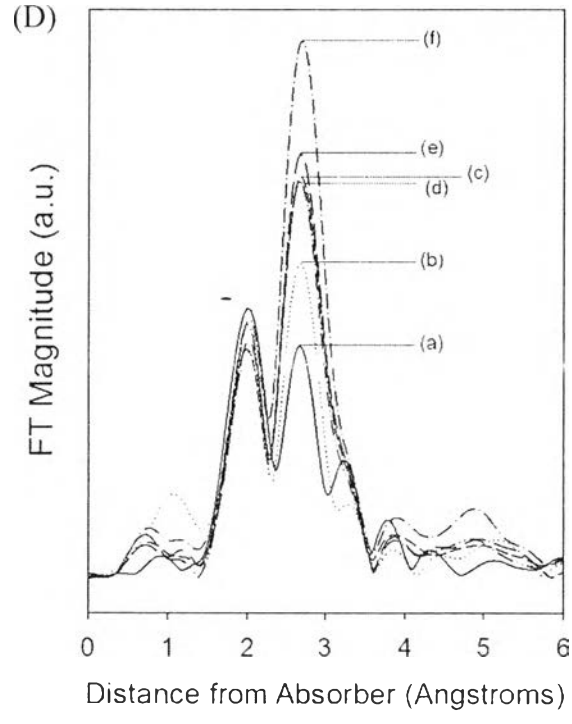

Figure 7.6 (A) k^1-Weighted EXAFS Fourier transform magnitude spectra of Ag promoted Co/Al_2O_3 catalysts and Ag reference compounds (not to scale), (B) TPR-EXAFS k^1-Weighted Fourier transform magnitude spectra of 2.76%Ag-25%Co/Al_2O_3, (D) k^1-weighted EXAFS Fourier transform magnitude spectra of Ag-promoted catalysts after TPR after cooling to ambient conditions: (a) raw $k^1 \cdot \chi(k)$ vs. k data; (b) filtered $k^1 \cdot \chi(k)$ vs. k data (solid line) and resulting fitting (filled circles); (c) Fourier transform magnitude spectra (solid line), and first shell fitting (filled), moving downward. (I) 0.276%Ag-25%Co/Al_2O_3; (II) 0.553%Ag-25%Co/Al_2O_3; (III) 1.11%Ag-25%Co/Al_2O_3; (IV) 1.66%Ag-25%Co/Al_2O_3; (V) 2.21%Ag-25%Co/Al_2O_3; (VI) 2.76%Ag-25%Co/Al_2O_3. (C) k^1-Weighted Fourier transform magnitude spectra after the TPR after the catalysts were cooled to ambient conditions, (a) 0.276%Ag-25%Co/Al_2O_3; (b) 0.553%Ag-25%Co/Al_2O_3; (c) 1.11%Ag-25%Co/Al_2O_3; (d) 1.66%Ag-25%Co/Al_2O_3; (e) 2.21%Ag-25%Co/Al_2O_3; and (f) 2.76%Ag-25%Co/Al_2O_3.

Table 7.3 Results of EXAFS fitting parameters for references acquired near the Ag K-edge. The fitting ranges were approximately $\Delta k = 2\text{-}10$ Å^{-1} and $\Delta R = 1.5\text{-}3.1$ Å, $S_0^2 = 0.9$

Catalyst	N Ag-Co	R Ag-Co (Å)	N Ag-Ag	R Ag-Ag (Å)	$N_{Ag\text{-}Co}/N_{Ag\text{-}Ag}$	e_0 (eV)	σ^2 (Å^2)	r-factor
Ag foil	-	-	12	2.858 (0.0081)	-	0.370 (0.493)	0.0106 (0.0007)	0.015
Ag-Ag fitting only								
0.276%Ag-25%Co/Al_2O_3	-	-	6.6 (4.5)	2.764 (0.084)	-	-1.38 (3.48)	0.0277 (0.0178)	0.212
Ag-Co and Ag-Ag fitting								
0.276%Ag-25%Co/Al_2O_3	2.0 (0.46)	2.676 (0.017)	3.4 (0.59)	2.758 (0.018)	0.59	-1.92 (1.00)	0.0112 (0.0027)	0.022
0.553%Ag-25%Co/Al_2O_3	1.8 (0.46)	2.657 (0.018)	5.0 (0.64)	2.786 (0.014)	0.36	-0.879 (0.724)	0.0147 (0.0021)	0.016
1.11%Ag-25%Co/Al2O_3	1.8 (0.49)	2.649 (0.020)	7.2 (0.73)	2.810 (0.012)	0.25	-0.541 (0.582)	0.0169 (0.0019)	0.011
1.66%Ag-25%Co/Al_2O_3	1.8 (0.57)	2.663 (0.025)	6.7 (0.86)	2.804 (0.014)	0.27	-0.896 (0.751)	0.0155 (0.0023)	0.017
2.21%Ag-25%Co/Al_2O_3	1.7 (0.59)	2.660 (0.026)	7.4 (0.90)	2.817 (0.014)	0.23	-0.506 (0.691)	0.0164 (0.0022)	0.015
2.76%Ag-25%Co/Al_2O_3	1.4 (0.52)	2.667 (0.030)	8.7 (0.85)	2.829 (0.011)	0.16	-0.340 (0.570)	0.0155 (0.0017)	0.0098

7.4.5 Catalytic Testing

As demonstrated in the literature, adding either Pt or Ag promoter can significantly improve CO conversion on Co/Al_2O_3 catalyst on a per gram catalyst basis (Cook et al., 2012; Jacobs et al., 2009; Schanke et al., 1995; Wang et al., 1991). The enhancement in conversion rate after introducing metal promoter stresses that one primary role of promoters is to provide a higher Co metal active site density for carrying out the reaction. Note that not all metals found to promote reduction led to improved X_{co}; Cu was one metal that clearly promoted Co oxide reduction, but led to negative effects on both CO conversion and product selectivity (Jacobs et al., 2009). In addition to the aim of improving the reducibility of cobalt oxide and enhancing the CO conversion rate, it was also our intent to further investigate the possibility of decreasing the hydrogenating activity of Co with the aim of decreasing light products (e.g., CH_4) and CO_2 and thus increase liquid HC product selectivity (C_5+). Comparisons of product selectivity generated from Pt and Ag promoted catalysts were thus conducted at the same level of conversion. The CO conversion was set at ~50% (i.e., industrially relevant conditions) by adjusting space velocity as a basis of comparison. The influences of Pt and Ag promoter and loadings on product selectivities are summarized in Table 7.4.

For Pt promoted catalyst, it is obvious that Pt slightly increases the formation of CH_4 and CO_2 and decreases C_5+ as compared to the unpromoted catalyst at ~50% CO conversion. However, Pt promoter significantly increased the catalyst initial activity on a per gram catalyst basis, as indicated by the much higher space velocities (12-16 NL/g-cat/h) used to achieve ~50% CO conversion at the beginning of FTS for the 0.5-5%Pt promoted Co catalysts relative to the unpromoted $25\%Co/Al_2O_3$ catalyst (4.2 NL/g-cat/h). Considering the effect of Pt loading with time on stream (TOS), once CO_2, CH_4 and C_5+ selectivities were established, their changes with time on stream were unnoticeable. CO_2 selectivity was found to increase measurably (0.8%, 1.1%, and 3.2% for unpromoted, 0.5%Pt-promoted, and 5%Pt promoted, respectively) with increasing Pt loading. The catalysts deactivated with time, and the space velocity was adjusted to maintain ~50%CO conversion. Another interesting perspective is the effect of Pt loading on the activity of the catalyst on per gram basis. Considering space velocity adjustments, it is clear that

higher space velocities were applied in the case of higher Pt loading. This means that Pt does help to promote CO conversion per unit mass of catalyst. Nevertheless, the product selectivity does not remain the same, and Pt tends to contribute to higher CH_4 and, especially, to more CO_2. Consequently, another important conclusion to be drawn from this work is that while high levels of Pt loading are able to produce higher CO conversion, it comes at the expense of slight losses in favorable C_5+ selectivity. The remarkable increase in CO_2 selectivity with increasing Pt also suggests that the water-gas shift (WGS) reaction pathway is enhanced, as Pt metal likely serves as an active site for this reaction (Bunluesin et al., 1998; Grenoble et al., 1981; Kalamaras et al., 2008; Phatak et al., 2007), perhaps by facilitating the dehydrogenation of formate during steam-assisted forward formate decomposition (Jacobs et al., 2010). With higher water gas shift reaction rates, higher CO_2 and H_2 levels are obtained and, subsequently, the additional H_2 may accelerate the hydrogenation reaction on Co sites, thus obstructing the long chain HC growth on these sites, in agreement with the lower C_5+ selectivities and higher methane selectivity as mentioned previously. Higher CH_4 selectivity may be the result of a higher hydrogen surface pool as a result of a higher H_2 dissociation/spillover rate due to Pt. Another possibility is a slightly higher WGS rate (perhaps due to Pt/alumina species). A slightly higher CO_2 production rate was observed at high Pt loading which in turn indicates that a small amount of H_2 is likely formed by WGS. Therefore, in order to apply Pt as a promoter for Co/Al_2O_3 FT catalyst, CO conversion and product selectivities must be compromised, such that low Pt loadings are warranted, aside from the cost factor.

For Ag promoted catalyst, the result in selectivity is intriguing as Ag promoter was confirmed to lower the chain termination rate of Co, as a decrease in methane selectivity was obtained, and C_5+ HC product selectivity increased. CO_2 selectivity was also diminished, indicating that Ag metal inhibits CO_2 formation. This means that Ag metal inhibits the water gas shift (WGS) reaction, in contrast to Pt metal. With increasing Ag loading, initially the catalyst still performed with higher C_5+ selectivity in line with the lower loaded Ag promoted catalyst, but CH_4 and CO_2 selectivities tended to slightly increase during ~150 h of testing. Because local atomic structure shows that Ag-Co bond formation is favorable at lower

loading, it is suggested that this Ag-Co interaction may selectively inhibit some active sites for CH_4 and CO_2 formation, while at high Ag loading, silver tends to form more Ag metal clusters and thus higher Ag-Ag coordination; this tendency may result in sites for inhibiting CH_4 being lost with time on-stream for the more heavily Ag loaded catalysts. It has been previously reported that Ag-active metal alloys in catalysts for selective hydrogenation reactions of butadiene and acetylene do suppress hydrogenation reactions (Borodziński et al., 2008; Redjala et al., 2006). At longer times on stream, slight increases in CH_4 and CO_2 selectivities and slight decreases in C_5+ selectivity were observed for all loadings; however, the selectivities are still better than both the unpromoted catalyst as well as the Pt-promoted catalyst. To reiterate, the negative selectivity changes with TOS might be due to the segregation of Ag during the reaction that leads to the formation of a separate Ag metallic phase (Jacobs et al., 2009), while losing Ag-Co coordination that retards CH_4 and CO_2 formation. As with Pt promoted catalyst, the CO conversion of Ag promoted catalysts declined with TOS because Co active sites are lost by deactivation processes, which were not analyzed in this contribution, such that lower space velocities were required to retain the ~50% CO conversion level. Unlike the case of Pt promoter, increasing Ag loading decreased catalyst activity on a per gram catalyst basis, as clearly observed by the lower space velocity that was needed to make equivalent 50% CO conversion when higher loadings of Ag were applied. This suggests that Ag metal clusters dominating at high Ag loading impede access of reactants to Co active sites, either by pore blocking or covering of sites. Among different Ag loadings the best Ag loading was found to be the lowest level (0.276%Ag), providing the highest activity coupled with the highest C_5+ selectivity among all the catalysts tested.

To summarize thus far, although there was found a fundamental difference in the local atomic structure between Pt and Ag promoter in Co/Al_2O_3 catalysts, both are able to effectively catalyze the reduction of cobalt oxide and provide higher Co^0 site densities for the reaction relative to the unpromoted catalyst; moreover, they also provide good activity for the FT reaction with satisfactory selectivities, especially in the case of Ag that can slightly lower CH_4 and CO_2 formation and improve C_5+ product selectivities.

Table 7.4 Activity and selectivity of the Fischer-Tropsch synthesis reaction on unpromoted Co/Al_2O_3 catalyst compared to Pt and Ag promoted Co/Al_2O_3 catalysts [a]

Catalyst	TOS, h	CO conversion, %	Space velocity, $NL/g_{cat}/h$	Hydrocarbon selectivity, carbon atom %		CO_2 sel., carbon atom %
				CH_4	C_5+	
$25\%Co/Al_2O_3$						
	8.7-53	51.0	3.4-4.2	8.3	82.5	0.8
	53-145	51.4	2.8	8.9	80.0	0.9
$0.5\%Pt-25\%Co/Al_2O_3$						
	6.3-58	52.0	1.7-12	9.1	81.2	1.1
	58-121	48.2	1.1-1.7	10.9	78.9	1.4
$2.0\%Pt-25\%Co/Al_2O_3$						
	6.0 -58	45.0	9.0-12.0	9.1	81.9	1.1
	58-143	50.6	6.2-6.9	9.2	81.2	1.8
$5.0\%Pt-25\%Co/Al_2O_3$						
	6.0-55.0	52.5	10-16.0	9.5	80.7	3.2
	71-175	49.5	9.1-10	9.9	79.0	4.0
$0.276\%Ag-25\%Co/Al_2O_3$						
	6.0-48	46.4	8.8-12	7.4	84.1	0.4
	56-149	49.4	4.5-7.0	7.9	82.3	0.5
$1.11\%Ag-25\%Co/Al_2O_3$						
	6.0-48	48.1	8.3-12	7.3	83.7	0.4
	55-145	50.1	5.0-6.2	8.4	81.4	0.6
$2.76\%Ag-25\%Co/Al_2O_3$						
	6.0-46	44.5	7.0-12	7.6	84.1	0.6
	49-120	48.7	3.4-4.8	8.3	81.2	0.8

[a]Reaction conditions: 220 °C, 300 psig, $H_2/CO = 2.1$

7.5 Conclusion

A series of Pt loaded cobalt catalysts was prepared as a reference for comparing the effectiveness of Ag as a promoter, as it is much less costly. In agreement with our previous reports, Pt and Ag promoters do facilitate the reduction of cobalt oxides and improve the number of active Co metal surface sites. Although increasing Ag enhances Co reduction, in contrast to Pt the metal site density does not increase with further increase in loading. While it is known that Pt in Co/Al_2O_3 catalyst is in intimate contact at the atomic level with cobalt clusters, with Pt-Co bonds being readily observed, this work demonstrates that this holds true even at very high promoter loadings. Ag promoter can also interact with Co to form Ag-Co bond in Ag promoted Co/Al_2O_3 catalysts. However, unlike Pt promoter, Ag promoter also displays coordination to other Ag atoms and a peak for Ag-Ag first shell coordination after complete activation in H_2 is evident. Moreover, the fraction of Ag in coordination with Co decreases as a function of Ag promoter loading, revealing that the interaction of silver with cobalt is not as high as in the case of platinum. While either Pt-Co bonds or Ag-Co bonds formed in Co/Al_2O_3 can significantly facilitate the reduction of cobalt oxides, the fundamentally different atomic structure of the Ag promoter relative to Pt plays a different role in product selectivity of the Fischer-Tropsch synthesis reaction. Pt promoter increases CH_4 and CO_2, at the expense of C_5+. The greater the amount of Pt, the higher CH_4 and CO_2 selectivities. Water gas shift (WGS) activity of Pt is at least in part responsible for the adverse effect. Interestingly, compared to both Pt promoted and unpromoted catalysts, Ag promoter at all loadings decreases CH_4 and CO_2 and benefits C_5+ selectivity. However, increasing Ag does not improve selectivity but rather worsens it relative to lower loadings, which may be attributed losses in Ag-Co bonding that inhibits excessive hydrogenation and/or WGS. Despite a somewhat lower performance for promoting Co metal site density relative to Pt, the satisfactory activity and higher selectivity obtained with Ag promoter and, in particular, its much lower price relative to Pt, makes Ag an important candidate as a possible substitute.

7.6 Acknowledgments

CAER work was supported by a NASA grant (Relating FTS catalyst properties to performance No. NNX11AI75A) and by the Commonwealth of Kentucky. Argonne's research was supported in part by the U.S. DOE, Office of Fossil Energy, NETL. The use of the APS was supported by the U.S. DOE, Office of Science, Office of Basic Energy Sciences, under Contract No. DE-AC02-06CH11357. MRCAT operations are supported by the DOE and the MRCAT member institutions. We would like to thank Ms. Shelly Hopps for her assistance with XRD experiments. We are also grateful to the Fulbright-TRF scholarship program for financial support for Mr. Thani Jermwongratanachai.

7.7 References

Arnoldy, P., and Moulijn, J.A. (1985) Temperature-programmed reduction of CoO Al_2O_3 catalysts. Journal of Catalysis, 93(1), 38-54.

Borodziński, A. and Bond, G.C. (2008) Selective hydrogenation of ethyne in ethene-rich streams on palladium catalysts, Part 2: steady-state kinetics and effects of palladium particle size, carbon monoxide, and promoters. Catalysis Reviews - Science and Engineering, 50(3), 379-469.

Bunluesin, T., Gorte, R.J., and Graham, G.W. (1998) Studies of the water-gas-shift reaction on ceria-supported Pt, Pd, and Rh: implications for oxygen-storage properties. Applied Catalysis B: Environmental, 15(1-2), 107-114.

Christensen, S.T., Elam, J.W., Rabuffetti, F.A., Ma, Q., Weigand, S.J., Lee, B., Seifert, S., Stair, P.C., Poeppelmeier, K.R., Hersam, M.C., and Bedzyk, M.J. (2009) Controlled growth of platinum nanoparticles on strontium titanate nanocubes by atomic layer deposition. Small, 5(6), 750-757.

Cook, K.M., Poudyal, S., Miller, J.T., Bartholomew, C.H., and Hecker, W.C. (2012) Reducibility of alumina-supported cobalt Fischer–Tropsch catalysts: effects of noble metal type, distribution, retention, chemical state, bonding, and influence on cobalt crystallite size. Applied Catalysis A: General, 449, 69-80.

Cronauer, D.C., Elam, J.W., Kropf, A.J., Marshall, C.L., Gao, P., Hopps, S., Jacobs, G., and Davis, B.H. (2012) Fischer–Tropsch synthesis: preconditioning effects upon Co-containing promoted and unpromoted catalysts. Catalysis Letters, 142(6), 698-713.

Das, T.K., Jacobs, G., Patterson, P.M., Conner, W.A., Li, J., and Davis, B.H. (2003) Fischer-Tropsch synthesis: Characterization and catalytic properties of rhenium promoted cobalt alumina catalysts. Fuel, 82(7), 805-815.

Espinoza, R.L., Visagie, J.L., Van Berge, P.J., Bolder, F.H. (1998). US Patent 5,733,839.

Greenwood, N.N., Earnshaw, A. (1997) Chemistry of the Elements. 2nd ed., Oxford: Butterworth Heinemann, pp. 1116.

Grenoble, D.C., Estadt, M.M., and Ollis, D.F. (1981) The chemistry and catalysis of the water gas shift reaction. 1. The kinetics over supported metal catalysts. Journal of Catalysis, 67(1), 90-102.

Guczi, L., Bazin, D., Kovács, I., Borkó, L., Schay, Z., Lynch, J., Parent, P., Lafon, C., Stefler, G., Koppány, Z., and Sajó, I. (2002) Structure of Pt-Co/Al_2O_3 and Pt-Co/NaY bimetallic catalysts: Characterization by in situ EXAFS, TPR, XPS and by activity in Co (carbon monoxide) hydrogenation. Topics in Catalysis, 20(1-4), 129-139.

Hilmen, A.M., Schanke, D., and Holmen, A. (1996) TPR study of the mechanism of rhenium promotion of alumina-supported cobalt Fischer-Tropsch catalysts. Catalysis Letters, 38(3-4), 143-147.

Jacobs, G., and Davis, B.H. (2010) Surface interfaces in low temperature water-gas shift: The metal oxide synergy, the assistance of co-adsorbed water, and alkali doping. International Journal of Hydrogen Energy, 35(8), 3522-3536.

Jacobs, G., Chaney, J.A., Patterson, P.M., Das, T.K., Maillot, J.C., and Davis, B.H. (2004) Fischer-Tropsch synthesis: Study of the promotion of Pt on the reduction property of Co/Al_2O_3 catalysts by in situ EXAFS of Co K and Pt LIII edges and XPS. Journal of Synchrotron Radiation, 11(5), 414-422.

Jacobs, G., Das, T.K., Zhang, Y., Li, J., Racoillet, G., and Davis, B.H. (2002) Fischer–Tropsch synthesis: support, loading, and promoter effects on the

reducibility of cobalt catalysts. Applied Catalysis A: General, 233(1–2), 263-281.

Jacobs, G., Ji, Y., Davis, B.H., Cronauer, D., Kropf, A.J., and Marshall, C.L. (2007) Fischer–Tropsch synthesis: Temperature programmed EXAFS/XANES investigation of the influence of support type, cobalt loading, and noble metal promoter addition to the reduction behavior of cobalt oxide particles. Applied Catalysis A: General, 333(2), 177-191.

Jacobs, G., Ribeiro, M.C., Ma, W., Ji, Y., Khalid, S., Sumodjo, P.T.A., and Davis, B.H. (2009) Group 11 (Cu, Ag, Au) promotion of 15%Co/Al2O3 Fischer–Tropsch synthesis catalysts. Applied Catalysis A: General, 361(1–2), 137-151.

Jacobs, G., Zhang, Y., Das, T.K., Li, J., Patterson, P.M., and Davis, B.H. (2001). Deactivation of a Ru promoted Co/Al_2O_3 catalyst for FT synthesis. In Spivey, J.J., Roberts, G.W., Davis, B.H. (Eds.), Catalyst deactivation 2001: proceeding of the 9th international symposium (pp. 415-422). Amsterdam: Elsevier.

Jacoby, M. (2001). X-ray absorption spectroscopy. Chemical and Engineering News, 79(32), 33-38.

Kalamaras, C.M., Olympiou, G.G., and Efstathiou, A.M. (2008) The water-gas shift reaction on Pt/γ-Al_2O_3 catalyst: Operando SSITKA-DRIFTS-mass spectroscopy studies. Catalysis Today, 138(3–4), 228-234.

Kinoshita, K. (1977) Differential thermal analysis of PtO_2/carbon. Thermochimica Acta, 20(3), 297-308.

Kogelbauer, A., Goodwin Jr, J.G., and Oukaci, R. (1996) Ruthenium promotion of Co/Al_2O_3 Fischer-Tropsch catalysts. Journal of Catalysis, 160(1), 125-133.

Kuzmin, A., Dalba, G., Fornasini, P., Rocca, F., and Šipr, O. (2006) X-ray absorption spectroscopy of strongly disordered glasses: Local structure around Ag ions in g-Ag_2O-nB_2O_3. Physical Review B - Condensed Matter and Materials Physics, 73(17), 174110-1-174110-12.

Newville, M., Ravel, B., Haskel, D., Rehr, J.J., Stern, E.A., Yacoby, Y. (1995) Analysis of multiple-scattering XAFS data using theoretical standards. Physica B: Condensed Matter, 208-209, 154-156.

Phatak, A.A., Koryabkina, N., Rai, S., Ratts, J.L., Ruettinger, W., Farrauto, R.J., Blau, G.E., Delgass, W.N., and Ribeiro, F.H. (2007) Kinetics of the water–gas shift reaction on Pt catalysts supported on alumina and ceria. Catalysis Today, 123(1–4), 224-234.

Ravel, B. (2001) ATOMS: Crystallography for the X-ray absorption spectroscopies. Journal of Synchrotron Radiation, 8(2), 314-316.

Redjala, T., Remita, H., Apostolescu, G., Mostafavi, M., Thomazeau, C., and Uzio, D. (2006) Bimetallic Au-Pd and Ag-Pd clusters synthesised by γ or electron beam radiolysis and study of the reactivity/structure relationships in the selective hydrogenation of buta-1,3-diene. Oil and Gas Science and Technology, 61(6), 789-797.

Rehr, J.J., Albers, R.C., and Zabinsky, S.I. (1992) High-order multiple-scattering calculations of x-ray-absorption fine structure. Physical Review Letters, 69(23), 3397-3400.

Ressler, T. (1997) WinXAS97. Version 1.0.

Rønning, M., Nicholson, D.G., and Holmen, A. (2001) In situ EXAFS study of the bimetallic interaction in a rhenium-promoted alumina-supported cobalt Fischer-Tropsch catalyst. Catalysis Letters, 72(3-4), 141-146.

Schanke, D., Vada, S., Blekkan, E.A., Hilmen, A.M., Hoff, A., and Holmen, A. (1995) Study of Pt-Promoted Cobalt CO Hydrogenation Catalysts. Journal of Catalysis, 156(1), 85-95.

Sexton, B.A., Hughes, A.E., and Turney, T.W. (1986) An XPS and TPR study of the reduction of promoted cobalt-kieselguhr Fischer-Tropsch catalysts. Journal of Catalysis, 97(2), 390-406.

Vada, S., Hoff, A., ÅdnaneS, E., Schanke, D., and Holmen, A. (1995) Fischer-Tropsch synthesis on supported cobalt catalysts promoted by platinum and rhenium. Topics in Catalysis, 2(1-4), 155-162.

Van Berge, P.J., Barradas, S., Van De Loodsrecht, J., and Visagie, J.L. (2001) Advances in the cobalt catalyzed Fischer-Tropsch synthesis. Erdoel Erdgas Kohle, 117(3), 138-142.

Wang, W.-J., and Chen, Y.-W. (1991) Influence of metal loading on the reducibility and hydrogenation activity of cobalt/alumina catalysts. Applied Catalysis, 77(2), 223-233.

Weaver, J.F., Chen, J.-J., and Gerrard, A.L. (2005) Oxidation of Pt(111) by gas-phase oxygen atoms. Surface Science, 592(1-3), 83-103.